Dalton Transactions

ROYAL SOCIETY OF CHEMISTRY

PERSPECTIVE

View Article Online
View Journal | View Issue

Cite this: *Dalton Trans.*, 2026, **55**, 5090

Monocoordinated nitrenes and heavier pnictinidenes: transient to bottleable compounds

Sandeep Kumar, [a] Kanishk Tomer, [b] Avnish Singh [c] and Priyabrata Ghana *[d]

Received 16th December 2025,
Accepted 27th January 2026

DOI: 10.1039/d5dt02995c

rsc.li/dalton

Nitrenes (N–R) and heavier pnictinidenes (Pn–R; Pn = P–Bi, R = anionic substituents), which are monovalent group 15 elements, have long been regarded as fleeting reactive intermediates in organic chemistry, with their existence typically confirmed only under matrix isolation conditions. The past few years have witnessed a striking evolution of these species from ephemeral curiosities into isolable, well-defined compounds under ambient laboratory conditions, irrespective of their singlet or triplet ground states. This perspective provides a chronological review of recent advances in the counterintuitive chemistry of nitrenes and pnictinidenes in the condensed phase, including their diverse synthetic methodologies and unusual bonding and structural features.

1. Introduction

Reactive intermediates play a crucial role in shaping the foundation of modern chemistry, serving as key entities in mechanistic pathways and fundamental chemical processes.[1] While earlier investigations of these short-lived, high-energy species relied on gas-phase matrix isolation, the meticulous application of electronic and steric stabilization techniques in recent years has enabled their successful isolation. Carbon-centred reactive intermediates such as carbocations (R_3C^+), carbanions (R_3C^-), tertiary carbon radicals ($R_3C^\bullet$), and divalent carbenes (R_2C:) have been extensively investigated in the con-

[a]*Fakultät für Chemie und Chemische Biologie, Technische Universität Dortmund, Otto-Hahn-Straße 6a, 44227 Dortmund, Germany. E-mail: sandeep.kumar@tu-dortmund.de*
[b]*Max-Planck-Institut für Kohlenforschung, Kaiser-Wilhelm-Platz 1, 45470 Mülheim/Ruhr, Germany. E-mail: tomer@kofo.mpg.de*
[c]*Institut für Anorganische Chemie, Universität Bonn, Gerhard-Domagk-Str. 1, 53121 Bonn, Germany. E-mail: asingh@uni-bonn.de*
[d]*Indian Institute of Technology Gandhinagar (IITGN), Palaj Village, Gandhinagar, 382355 Gujarat, India. E-mail: priyabrata.ghana@iitgn.ac.in*

Sandeep Kumar

Dr Sandeep Kumar acquired his Bachelor of Science degree in 2017 from the esteemed University of Delhi, India. Following this, he successfully completed his Master of Science in 2019 at the prestigious Indian Institute of Technology Kanpur, India. Subsequently, in 2020, he embarked on an academic and research journey (PhD) at the Institute for Inorganic Chemistry, University of Bonn, Germany, under the supervision of Prof. A. C. Filippou, and completed it in 2025. Currently, he is working as a postdoctoral fellow at the Technical University of Dortmund. His scholarly interests are concentrated on the conceptualisation and synthesis of low-coordinate silicon and germanium compounds with unusual bonding motifs.

Kanishk Tomer

Dr Kanishk Tomer obtained his Bachelor of Science degree in 2018 from the University of Delhi, India, and his Master of Science degree in 2020 from the Indian Institute of Technology Kanpur (IITK), India. He commenced his doctoral studies in 2020 under the supervision of Prof. Dr Alexander C. Filippou at the Institute for Inorganic Chemistry, University of Bonn, Germany, and completed his PhD in 2025. He is currently a postdoctoral researcher at the Max Planck Institute for Coal Research (MPI für Kohlenforschung), Germany. His research centers on the development of innovative synthetic methodologies enabling the isolation of highly reactive low-valent Group 14 species, with particular emphasis on metal–tetrel triple bonds.

densed phase.[1] Though considerable effort has been directed toward the isolation of heavier Group 14 congeners, advancements in Group 15 pnictogen chemistry, particularly in the condensed-phase characterization of pnictogen-centered reactive intermediates, remain comparatively underdeveloped. Among them, Lewis base-free nitrenes R–N and heavier pnictinidenes Pn–R (Pn = P–Bi) comprise low-valent neutral monosubstituted pnictogen centres in the formal oxidation state of +1. Pnictinidenes consist of a pnictogen centre with a single σ-bonded substituent, resulting in an incomplete valence shell and rendering them highly reactive.[2,3] The valence shell can adopt a singlet or triplet electronic ground state, as illustrated in Fig. 1a. The singlet state configuration is characterized by two lone pairs and an empty p-orbital oriented perpendicular to the R–N or R–Pn bond. In contrast, the triplet configuration features one lone pair and two singly occupied p-orbitals, both perpendicular to the R–N or R–Pn bond.[4] *Ab initio* calculations indicate that π-donating substituents attached to the pnictogen atom significantly stabilize the singlet ground state, whereas σ-type ligands favour the triplet ground state.[5,6] These highly reactive electron-deficient species have found many applications in synthetic chemistry, such as CH-insertion, ring expansion, and aziridination processes.[7]

Nitrenes and heavier pnictinidenes, particularly in the context of transition metals, have been extensively explored and are frequently referred to as metallonitrenes or metal-nitrido complexes (L_nMN, where L_n is a ligand sphere and M is a transition metal),[8–14] and their heavier pnictinidene counterparts are commonly described as transition-metal terminal pnictide (L_nMPn) complexes because one of their leading resonance structures features metal–pnictogen multiple bonds (Fig. 1b).[15–23] Despite having an isoelectronic relation with carbenes, nonmetallic nitrenes and pnictinidenes exhibit substantial challenges for isolation due to their inherent inclination towards self-aggregation,[24–35] often necessitating stabilization through complexation with Lewis acids or bases.[36–40]

This perspective will chronologically explore groundbreaking developments in the unconventional chemistry of condensed-phase mono-coordinated pnictogens, systematically transitioning from transient intermediates to isolable, stable species.

2. Nitrenes: elusive intermediates to bottleable compounds

2.1. Matrix and low-temperature characterization of nitrenes

Nitrene-mediated transformations constitute one of the most versatile and potent methodologies for synthesising nitrogen-containing molecular skeletons.[1,41] While the parent nitrene (HN) has been observed only in interstellar space, Tiemann and coworkers first introduced nitrenes as transient intermediates in the Lossen rearrangement in 1891.[42,43] Early work highlighted the highly reactive nature of nitrenes, which is reflected in the extremely short lifetimes of arylnitrenes at ambient temperature, typically on the order of nanoseconds. Due to the high reactivity of these transient species, their behaviour has been largely inferred from matrix-trapping experiments at low temperatures, time-resolved spectroscopy, and quantum-chemical computations.[44,45] Nitrenes are commonly generated *via* FVP or photolysis and investigated under matrix-isolation conditions. Consequently, triplet ground-state arylnitrenes generated by FVP have been isolated in argon matrices and characterized using ESR spectroscopy.[46] For example, the triplet ground-state difluorophosphorylnitrene $F_2P(O)N$ (**2**) was synthesized *via* FVP of the corresponding azide $F_2P(O)N_3$ (**1**) and detected using matrix IR spectroscopy (Scheme 1a).[47] Theoretical calculations suggested a barrier of ~141 kJ mol^{-1}

Avnish Singh

Avnish Singh received his Bachelor of Science (Honours) degree in 2017 from the University of Delhi and his Master of Science degree in 2019 from the Indian Institute of Technology Kanpur, India. Following his postgraduate studies, he served as a Faculty Member in Chemistry at Roa Edusolution Pvt. Ltd for two years. In 2021, he commenced his doctoral studies under the supervison of Prof. Dr Alexander C. Filippou at the Institute of Inorganic Chemistry, University of Bonn, Germany. His research focuses on the synthesis, structural characterization, and reactivity of low-valent Group 14 species, with particular emphasis on elucidating their bonding motif and reactivity patterns in the context of main-group chemistry.

Priyabrata Ghana

Dr. Priyabrata Ghana received his PhD from the University of Bonn, Germany, where he worked with Prof. Alexander C. Filippou on main group-organometallic chemistry. After finishing his PhD, he moved to RWTH Aachen to work with Prof. Jun Okuda as a Postdoctoral Fellow. After spending nearly 3 years in Aachen, he moved to the USA to work with Prof. Theodor Agapie at the California Institute of Technology (Caltech), where he worked on the coordination copolymerization of ethylene and acrylates. Currently, Dr. Priyabrata Ghana is an Assistant Professor at the Indian Institute of Technology Gandhinagar, where his group is working on small molecule activation chemistry.

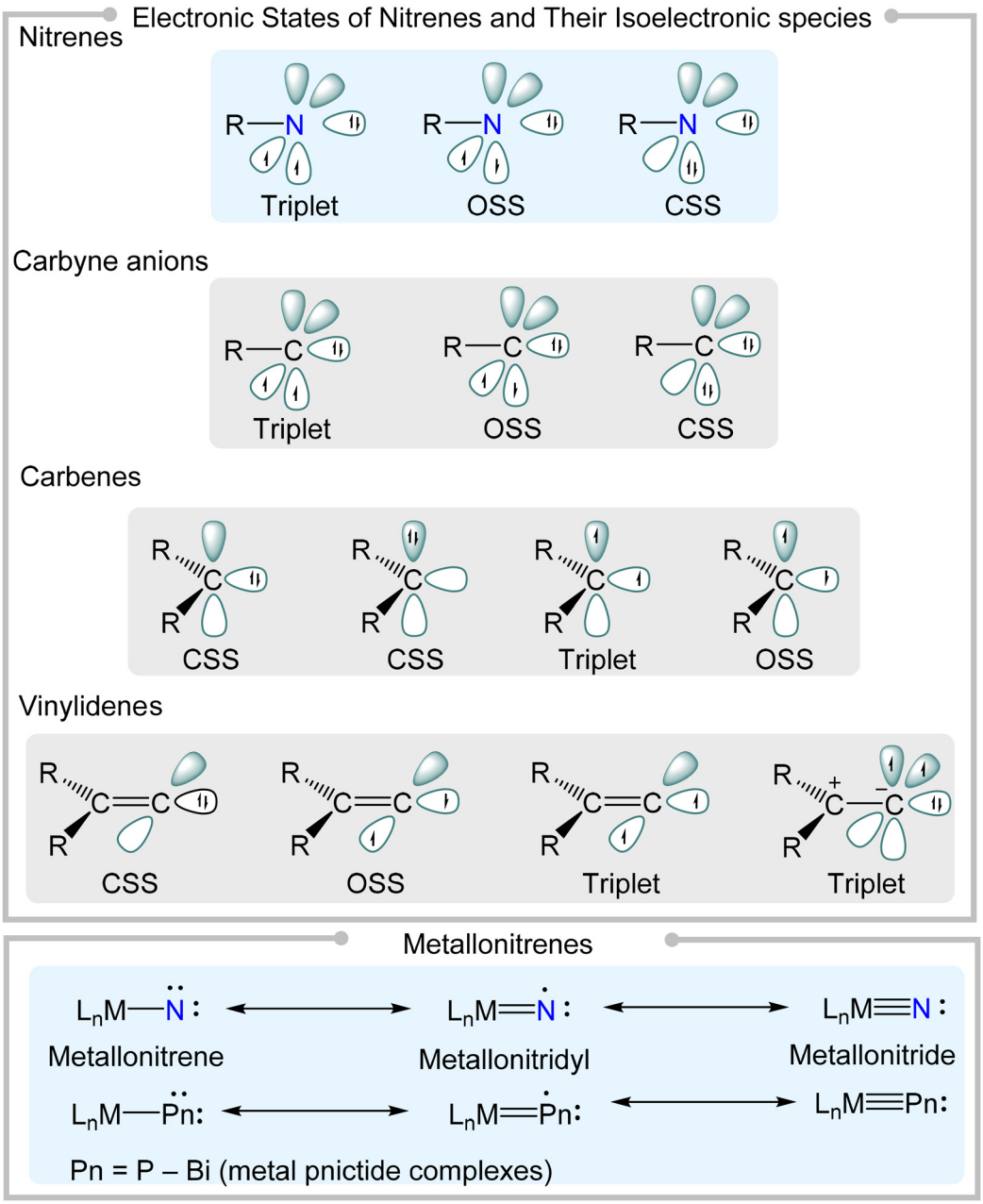

Fig. 1 Depiction of the electronic configurations of free nitrenes, carbyne anions, carbenes, and vinylidenes, showing triplet, open-shell singlet (OSS), and closed-shell singlet (CSS) states; metallonitrenes or metal–nitrido complexes[8–14] (top) and metal pnictide complexes[15–23] (bottom).

for the unobserved Curtius-type rearrangement to FP(O)═N–F, while a photochemical rearrangement to F_2P–N═O (**3**) was observed. The textbook "*Nitrenes: Reactive Intermediates in Organic Chemistry*" by W. Lwowski offers a comprehensive conceptual overview of foundational research in the discussed domain.[48]

Matrix photolysis of diazide (**4**) generated the triplet nitrene FP(O)(N_3)N (**5**), as identified by subsequent irradiation of the matrix-isolated photolysis products with near-UV visible light (λ_{max} > 335 nm) (Scheme 1b).[49] Both phosphorylnitrenes (**2** and **5**) have also been characterized by ESR and matrix IR spectroscopy.[50] Photolysis of the corresponding thiophosphoryl azide (**6**) resulted in the generation of the singlet ground-state nitrene $F_2P(S)N$ (**7**) (Scheme 1a). Upon FVP or irradiation with visible light, $F_2P(S)N$ (**7**) underwent rearrangement to yield the thionitroso isomer F_2P–N═S (**8**). Further irradiation of F_2P–N═S (**8**) at 365 nm reversed the reaction, leading to the regeneration of $F_2P(S)N$ (**7**) and isomerization to the thiazyl F_2P–S≡N (**9**) (Scheme 1a).[51]

The FVP of fluorosulfonyl azide FSO_3N_3 (**10**) generated fluorosulfonyl nitrene FSO_2N (**12**) in its triplet ground state as well, which was characterized by IR, UV/Vis, and ESR spec-

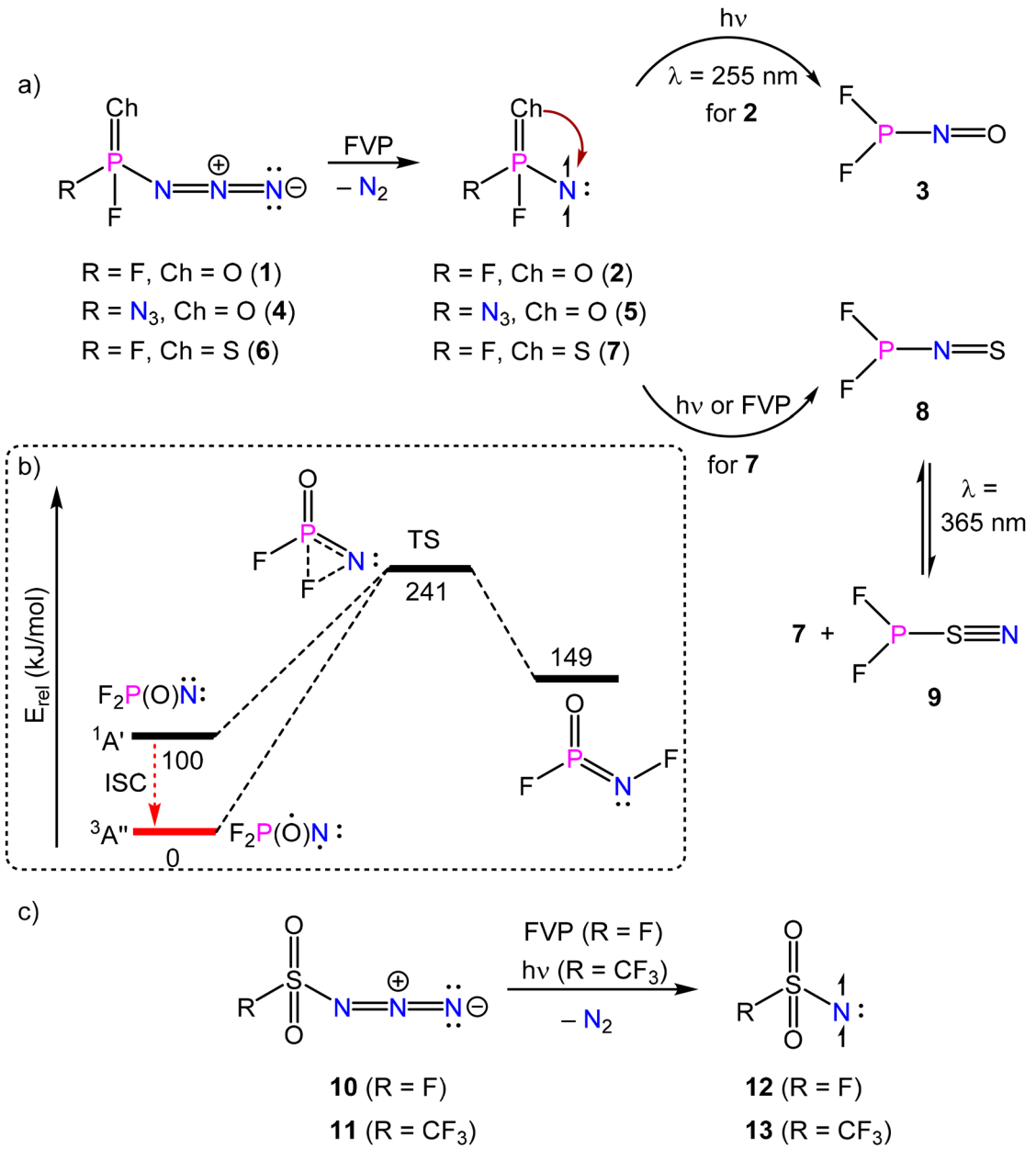

Scheme 1 (a) Matrix-isolation studies of ground-state triplet nitrenes.[47,49,50] (b) Calculated relative energies (kJ mol^{-1}) of the Curtius-type rearrangement for **2** at the B3LYP/6-311+G(3df) level of theory.[47] The ISC from the singlet (^{1}A′) to the triplet (^{3}A″) state of $F_2P(O)N$ is shown with a red arrowhead. (c) Matrix-isolation studies of ground-state triplet sulfonyl nitrenes.[52–54]

troscopy (Scheme 1c).[52,53] The fluorosulfonyl radical $FSO_2^{\bullet}$ was also formed during this process. While FVP of trifluoromethylsulfonyl azide $CF_3SO_2N_3$ (**11**) generated the radical $SO_2N^{\bullet}$,[54] the triplet ground-state nitrene CF_3SO_2N (**13**) was obtained *via* matrix photolysis (Scheme 1c). The matrix-isolated aforementioned nitrenes underwent Curtius-type rearrangements to afford $(R_1)NCh$ (R_1 = $CF_3(SO)$ and Ch = O, PF_2 (**3** (Ch = O) and **8** (Ch = S))).[55] Analogous reactions were observed for phenylsulfonyl nitrene, $PhSO_2N$.[56] In contrast, the sulfinyl nitrene CF_3SO–N exhibits a singlet ground state as a consequence of strong S–N interaction, which results in a thiazyne-like structure.[57]

Several triplet ground-state acylnitrenes X–CO–N, **15** and **18** (Scheme 2a and b),[58–61] including alkoxy- and aryloxycarbonylnitrenes **18** and **20** (Scheme 2b),[62,63] as well as carbamoylnitrenes R_2N–CO–N (**22**) (Scheme 2b),[64,65] have been synthesized *via* FVP or matrix photolysis of the corresponding azides (**14**, **19**, and **21**) or isocyanate precursors (**17**) and comprehensively characterized by IR and ESR spectroscopy. The chemistry and nature of singlet acylnitrenes R–CO–N are crucial due to their possible role in Curtius-type rearrangements, where acylazides transform into isocyanates. Notably, a recent review article by C. Wentrup provides a clear and comprehensive overview of

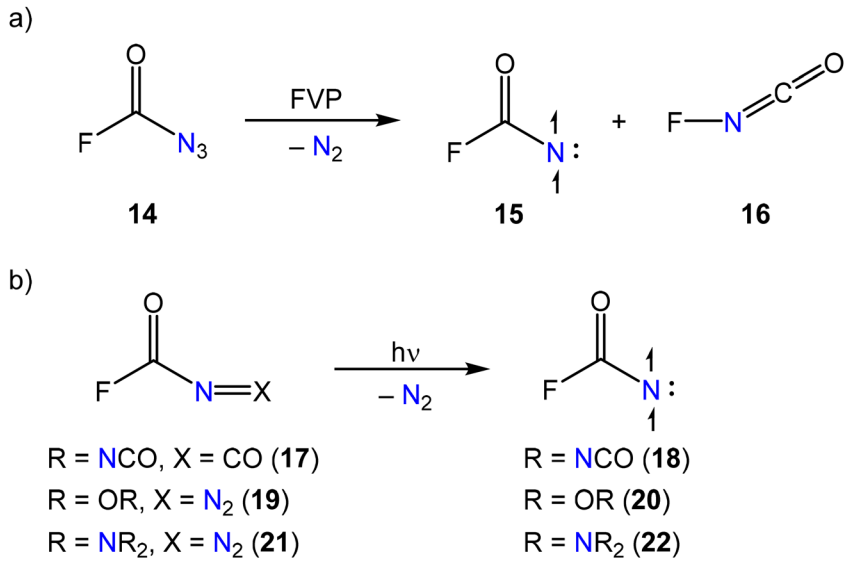

Scheme 2 Generation of triplet ground-state acylnitrenes,[57–60] alkoxy-and aryloxycarbonylnitrenes,[62,63] and carbamoylnitrenes.[64,65]

tunnelling in nitrene reactions, triplet and singlet acylnitrenes (oxazirines), bistable nitrenes, and in-depth studies of vinylnitrenes.[3]

Among the above-discussed non-metallic nitrenes, aminonitrenes represent the most stable class, owing to their electronic stabilization arising from donation of the amino-nitrogen lone pair into the symmetry-allowed vacant orbital of the nitrene (Scheme 3). This phenomenon, well captured by the 1,1-diazene resonance hybrid, closely resembles the stabilization paradigm long recognized in carbene chemistry.[66,67] Using the same concept, Dervan and coworkers demonstrated that *N*-(2,2,5,5-tetramethylpyrrolidyl)nitrene (**24**) and *N*-(2,2,6,6-tetramethylpiperidyl)nitrene (**26**) (Scheme 3a and b)[68–70] exhibit sufficient stability in solution at 195 K to enable comprehensive spectroscopic characterization and purification *via* low-temperature chromatography. However, due to their pronounced reactivity and short lifetimes, the isolation of base-free nitrenes in the condensed phase remains experimentally challenging.

2.2. Condensed-phase characterization of nitrenes

2.2.1. Singlet ground-state nitrenes. In 1980, Dervan and coworkers provided the primary indication of the condensed-phase characterization of base-free monocoordinated nitrenes.[70,71] As discussed earlier, this was achieved through electronic interaction between directly bonded π-donating substituents and the vacant p-orbital of the nitrene. Subsequently, Bertrand and coworkers interpreted conceptually that substituting the coordinating amino group on the nitrene atom with a phosphino group could further amplify the stabilization of nitrenes. In 2012, Bertrand and coworkers reported the successful isolation and characterisation of the unprecedented phosphinonitrene (**29**), exhibiting remarkable stability at ambient temperatures in both the solid and solution states.[7] The extra stabilization is attributed to back-donation of the nitrene lone pair into an energetically accessible σ* orbital on phosphorus. This was later corroborated by the theoretical calculations performed by Schoeller and coworkers, which eluci-

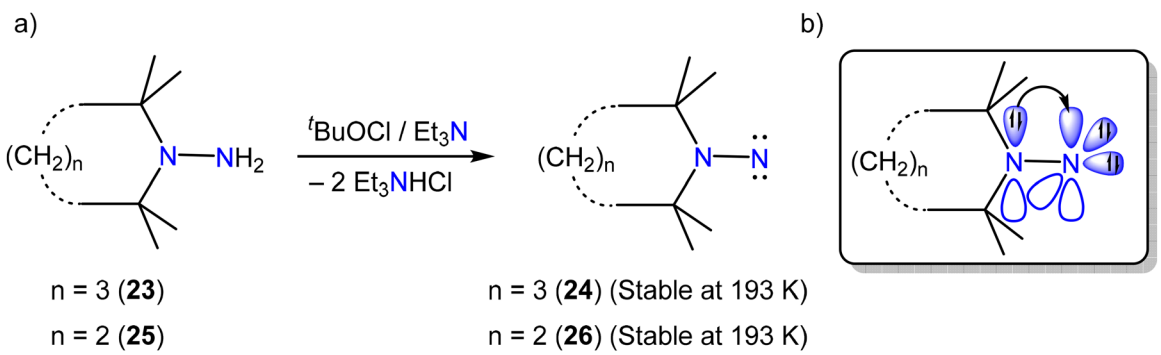

Scheme 3 (a) Singlet ground-state aminonitrenes **24** and **26**, stable at low temperature. (b) Interactions relevant to the stability of singlet aminonitrenes.[68,69]

dated that the optimal substituents for stabilizing phosphinonitrenes are characterized by potent π-donor and weak σ-acceptor properties at the α-position (*e.g.*, phosphaniminato functionalities).[72] Stephan and coworkers also demonstrated experimentally that electronically saturated organofluorophosphonium salts $[(C_6F_5)_{3-x}Ph_xPF][B(C_6F_5)_4]$ (x = 0 or 1) act as Lewis acids due to the availability of a σ*-acceptor orbital oriented trans to the fluoride substituent, thereby forming stable adducts with neutral Lewis bases.[73] The azide precursor (**28**) was isolated as colorless crystals in quantitative yield through a salt metathesis reaction between the corresponding chloride derivative (**27**) and NaN_3 (Scheme 4a). The $^{31}P\{^1H\}$ NMR spectrum of compound **28** exhibits a resonance at an upfield (δ_P = 111.0 ppm) relative to its chloride precursor **27** (δ_P = 276.3 ppm).[74] The azide formation could be traced by the upfield shifted resonance of **28**, and photolysis of a toluene solution of the azide under irradiation at λ = 254 nm, conducted at ambient temperature within a quartz reaction vessel, facilitated the generation of phosphinonitrene (**29**), accompanied by the liberation of N_2 (Scheme 4a).

Phosphinonitrene (**29**) exhibits diamagnetic characteristics according to NMR spectroscopy, and its ^{31}P NMR spectrum exhibits a significantly high-field-shifted singlet resonance (δ_P = 7.7 ppm) compared to that of its precursor **28** (δ_P = 111.0 ppm), a typical indication of a hypervalent phosphorus centre. The ^{15}N-enriched azide **28*** was synthesized from compound **27** and $Na^{15}NNN$ and subsequently photolyzed to yield the ^{15}N-enriched phosphinonitrene **29*** (Scheme 4b). Notably, the ^{15}N NMR spectrum of phosphinonitrene **29*** exhibits a doublet at δ_N = 266 ppm, with a significant P–N coupling constant ($^1J_{PN}$ = 144 Hz). In contrast, the azide precursor **28*** shows a doublet for N_α ($^1J_{PN}$ = 103 Hz) at δ_N = 95.8 ppm, which is upfield shifted compared to **29***. The higher coupling constant observed in **29*** suggests a stronger multiple bond character between phosphorus and the nitrene nitrogen ($P–N_{nitrene}$) in the phosphinonitrene, reinforcing the pronounced bonding interaction. Phosphinonitrene **29** is distinguished by a monocoordinated nitrogen atom and a nearly planar N_3P core (Fig. 2a). The monocoordinated nitrogen ($N7/N_{nitrene}$) is bonded to a perfectly trigonal planar phosphorus centre ($\Sigma\measuredangle(P)$ = 360°) with a short distance of 1.457(8) Å, which falls well within the expected range for a P=N double bond (1.50–1.60 Å).[75] The Wiberg bond index values corroborate the assignment of a double bond for P–N7 (2.09) and single bonds for P–N1 (0.85) and P–N4 (0.85), and align well with the crystallographic data. The lone pair on the phosphorus atom plays a crucial role in stabilizing the nitrene in its singlet ground state through lone-pair delocalization. DFT calculations performed on a closely related model compound $\mathbf{29_{m1}}$ (with a Ph group in place of the Dipp group) at the M05-2X/TZVPP level of theory revealed that the triplet-state configuration, characterized by pronounced pyramidalization of the phosphorus centre, is ener-

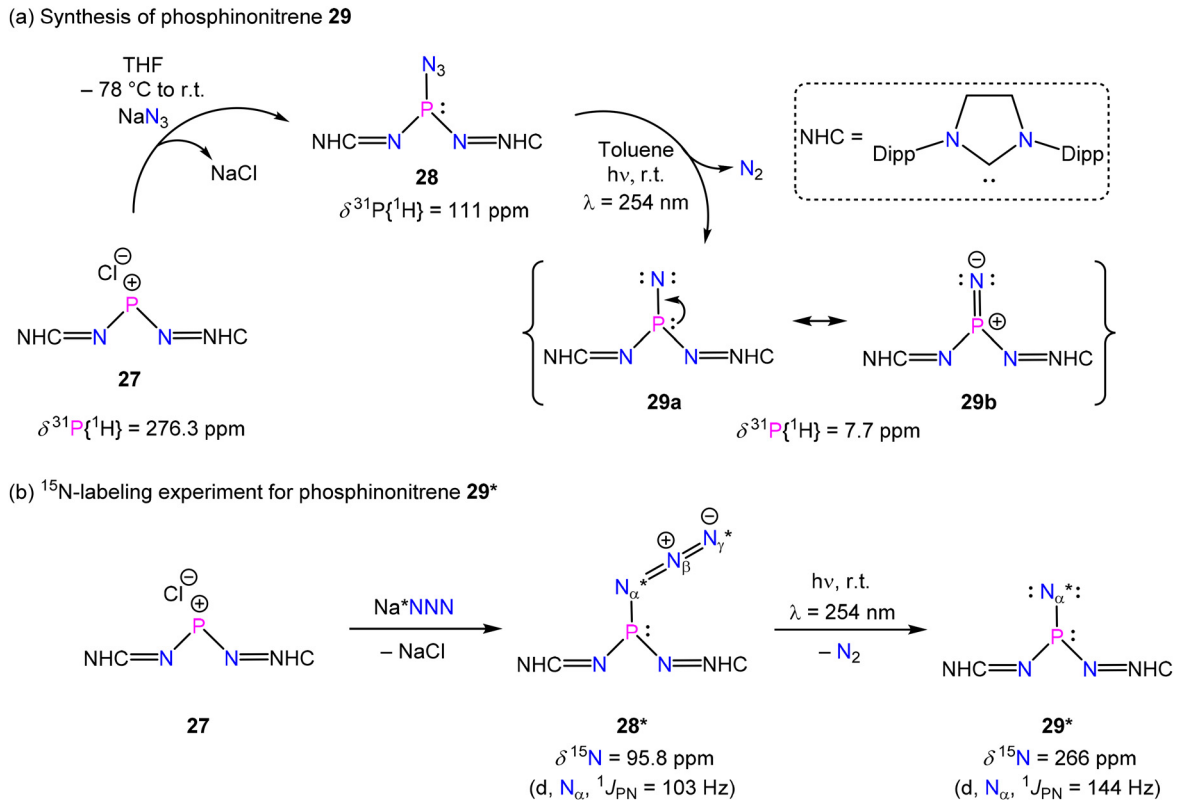

Scheme 4 (a) Synthesis of the unprecedented phosphinonitrene (**29**) upon irradiation of azide precursor **28**. (b) Synthesis and spectroscopic data for ^{15}N-labeled phosphinonitrene **29***.[7]

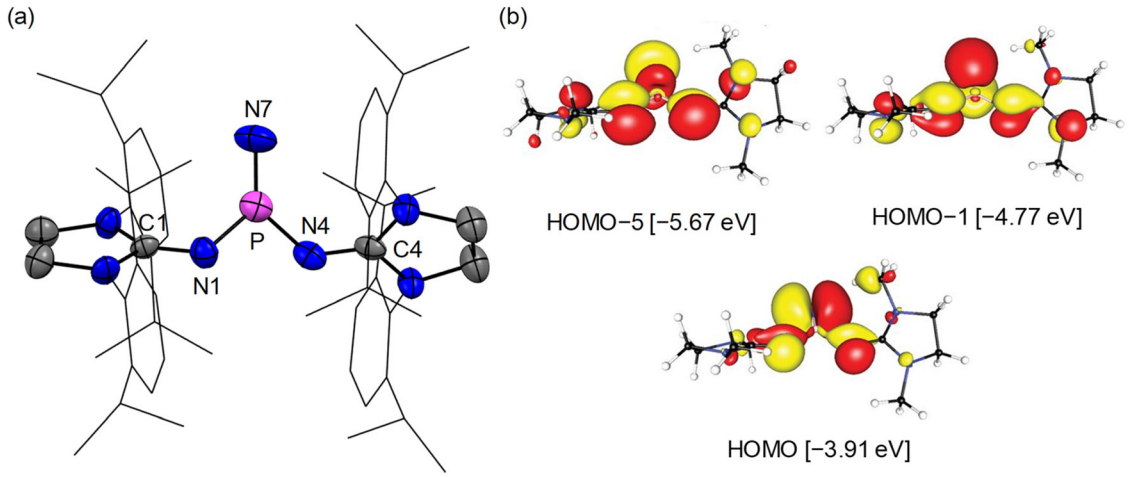

Fig. 2 (a) Molecular structure of singlet ground-state phosphinonitrene **29**; reproduced from ref. 7 with permission from the American Association for the Advancement of Science (AAAS), copyright © 2012. (b) Canonical molecular orbitals of $\mathbf{29_{m2}}$ calculated at the M05-2X/TZVPP level of theory, adapted from ref. 7 with permission from the American Association for the Advancement of Science (AAAS), copyright © 2012.

getically disfavored by 36 kcal mol^{-1} compared to the singlet ground state (Fig. 11).[7] The shapes of the canonical molecular orbitals of another closely related phosphinonitrene, $\mathbf{29_{m2}}$ (with a Me group in place of the Dipp group), show that the HOMO consists of an in-plane $\pi_{\|}$ lone-pair orbital at N7, whereas the HOMO−1 is a polarized out-of-plane P–N7 $\pi_{\perp}$ orbital, and the HOMO−5 is mainly a P–N7 σ-bonding orbital (Fig. 2b).

The electrophilic character of phosphinonitrene **29** enables the selective addition of ^{i}PrNC to the nitrene nitrogen ($N_{nitrene}$), resulting in the formation of the corresponding carbodiimide **30**. Notably, subsequent treatment of carbodiimide **30** with ^{i}PrOTf facilitates N-atom transfer from the nitrene moiety, culminating in the generation of phosphenium salt **33** alongside a mixture of cyanamide **32** and carbodiimide **31** (Scheme 5). This synthetic cycle underscores the exceptional capacity of phosphinonitrene **29** to mimic the reactivity paradigms typically associated with transition-metal chemistry.

2.2.2. Triplet ground-state metallonitrenes. Metal–ligand multiple-bonded complexes are pivotal catalytic intermediates in biological and synthetic chemistry,[76] where the reactivity as well as selectivity of substrate functionalization is heavily dependent on the electronic structure of these complexes.[10] Early transition-metal complexes with fewer d-electrons are stabilized by significant metal–ligand π-bonding. Due to strong π-donation from ligands, these complexes, such as oxo and nitrido species, are routinely isolated and characterized.[77] For early transition metals, the relative energies of metal- and ligand-centred orbitals give rise to ligand-based HOMOs.[78]

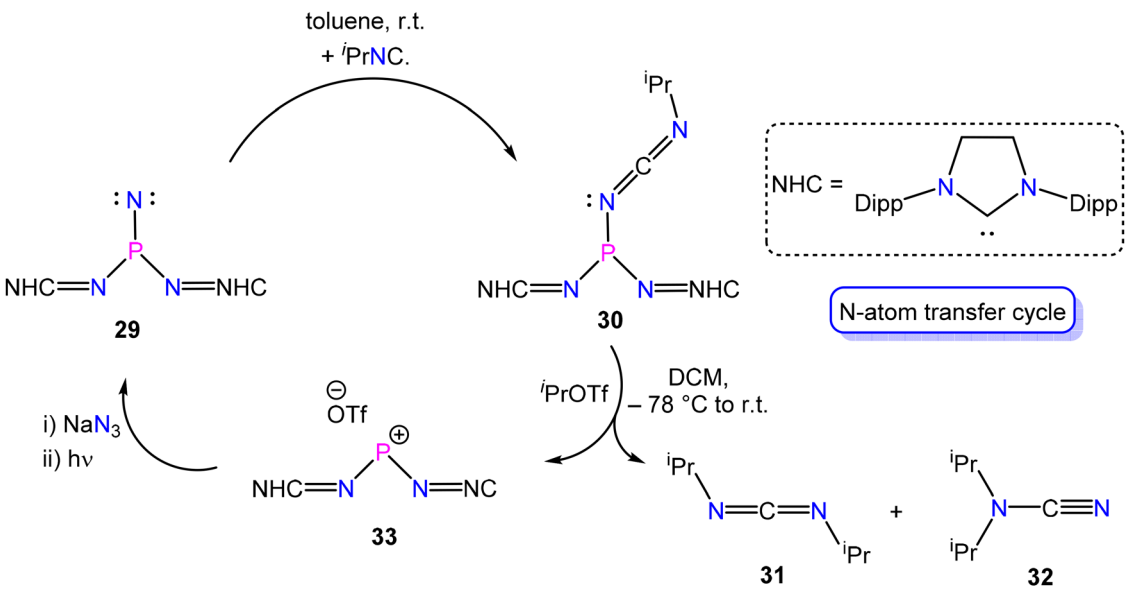

Scheme 5 Nitrogen atom-transfer synthetic cycle.[7]

However, for late transition metals, the energies of metal-centred orbitals decrease relative to ligand-centred orbitals, resulting in metal-centred HOMOs and ligand subvalence. In the context of terminal M–N, this progression from early to late transition metal series is accompanied by a progression from metal nitrides (trivalent nitrogen, M≡N) to metal nitridyl radicals (divalent nitrogen, M═N) and ultimately to metallonitrenes (monovalent nitrogen, M–N) (Fig. 3).[79] Ligand subvalence is associated with increased electrophilicity at nitrogen, which renders metallonitrenes powerful reactive intermediates for a variety of N-atom transfer reactions. However, the spectroscopic and structural characterization of authentic metallonitrenes (singlet or triplet ground states), featuring monovalent atomic nitrogen, remains relatively less explored. This long-standing void was effectively addressed by the seminal contributions of Holthausen, Schneider, and coworkers in 2020.[80]

The Pt(II) pincer azide complex [Pt(N$_3$)(PNP)] (PNP = N(CHCHP^{t}Bu$_2$)$_2$) (**34**) was selected as a platform for addressing this long-lasting gap in the field. The photolysis of Pt(II) azide complex **34**, irrespective of its physical state (solid or solution), with either a Xe arc lamp (λ_{exc} > 305 nm) or a violet LED (λ = 390 nm), indicated the formation of metallonitrene **35**. Complex **35** is highly reactive and was found to decompose at temperatures above 223 K in toluene and above 253 K in THF, which made solid-state isolation and crystallization significant challenges. Therefore, the structural characterization of metallonitrene **35** was performed using photocrystallography.[80] Photolysis of a single crystal of **34** with a 390 nm wavelength light-emitting diode irradiation at 100 K resulted in the formation of **35**. Photoconversion was evidenced by depletion of electron density in the region of the azide N$_\beta$ and N$_\gamma$ atoms and the observation of new electron density in a void space defined by the ^{t}Bu substituents of the ligand. Refinement of the resulting data set indicated 76% photoconversion of azide **34** to metallonitrene **35** (Scheme 6a). In 2022, the same research group disclosed the synthesis of the Pd–nitrene complex **37**,[81] accomplished by expanding the corresponding azide precursor **36**. The transformation was elucidated by photocrystallography, which confirmed the extrusion of N$_2$ in the crystal lattice (Scheme 6b). However, the presented metallonitrenes **35** and **37** are inherently unstable and cannot be isolated under ambient temperature conditions.

X-ray crystallographic analysis of complexes **35**[80] (Scheme 6b) and **37**[81] shows an isotypic skeletal arrangement characterized by an almost linear N$_{PNP}$–M–N$_{nitrene}$ bond axis (176.0(4)° (M = Pt) and 176.3(6)° (M = Pd)), with only slight perturbations noticed in the metallonitrene moieties relative to their corresponding azide precursor embedded within the M(PNP) scaffold. Furthermore, the process of N$_2$ elimination is associated with a pronounced contraction of the M–N$_{nitrene}$ bond length (Δd (Å) = 0.16 (Pt) and 0.14 (Pd)).

The electronic structures of both metallonitrenes were investigated using SQUID magnetometry and quantum-chemical calculations. The molar paramagnetic susceptibility–temperature product (χ^p_{mol}T) of the photogenerated products shows a linear dependence in the low-temperature region, eventually

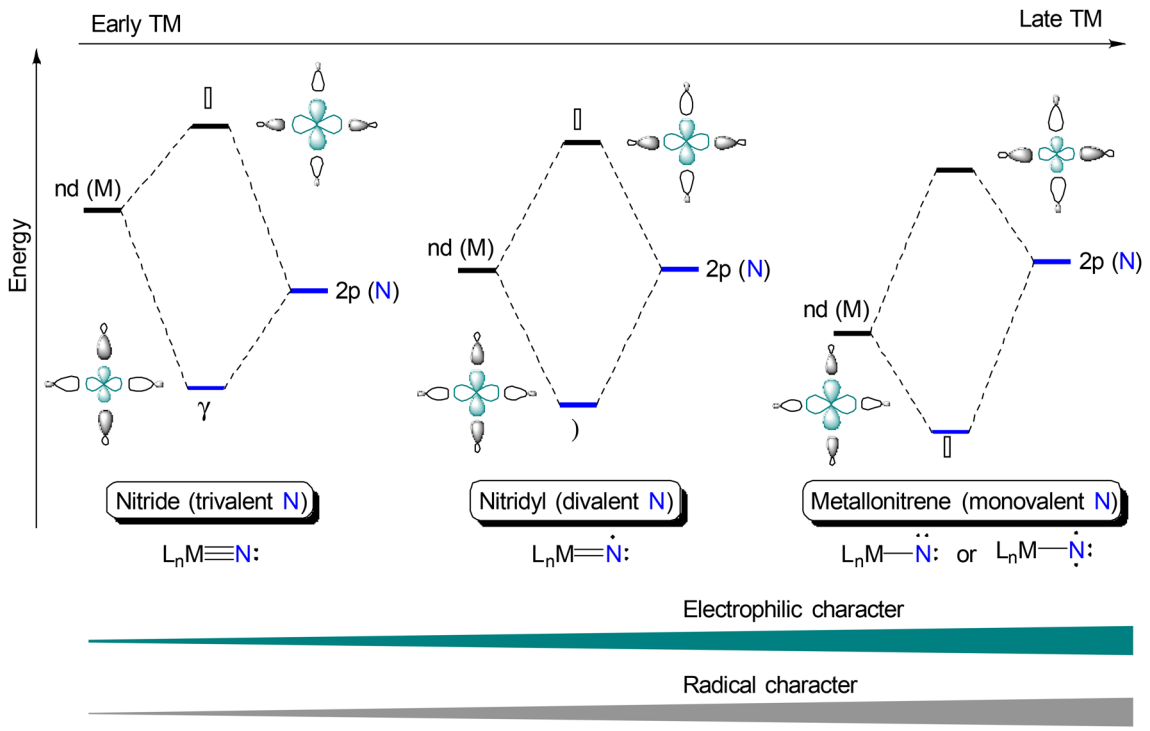

Fig. 3 The relative energies of the metal- and ligand-based orbitals give rise to nitride, nitridyl, and metallonitrene character as one moves from early to late transition metals (TM).[79]

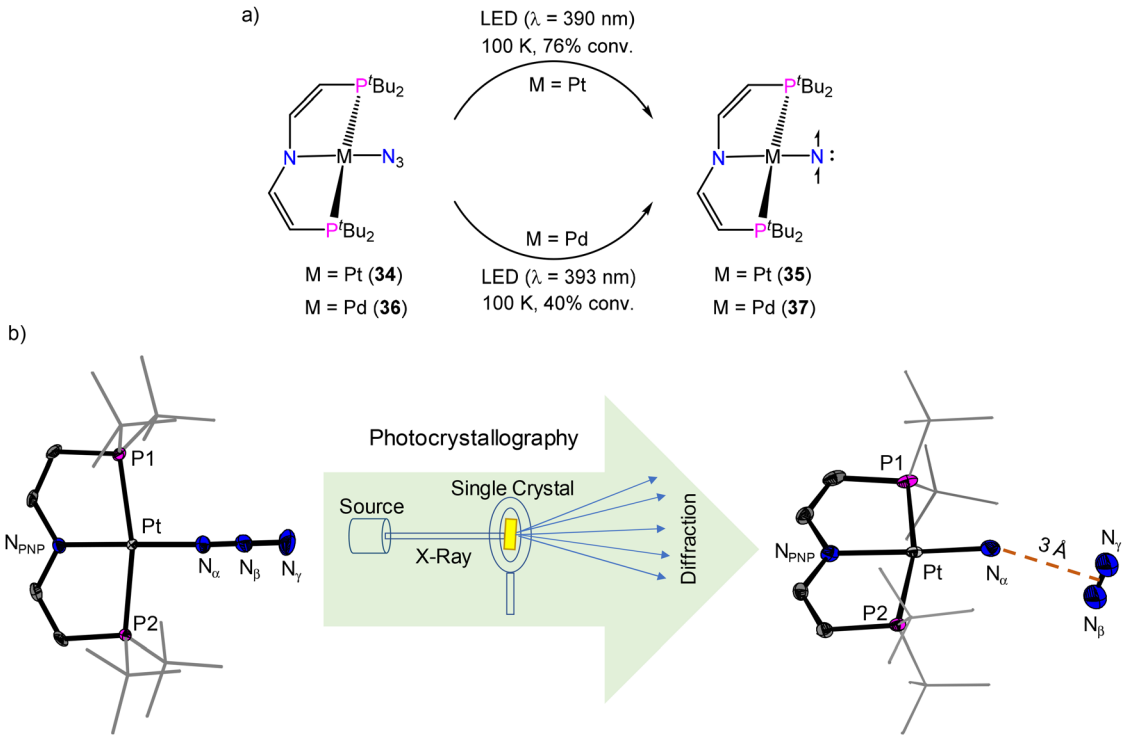

Scheme 6 (a) Photochemical synthesis of Pt and Pd metallonitrenes **35**[80] and **37**.[81] (b) Photocrystallography enabled structural characterization of thermally unstable metallonitrene **35**, reproduced from ref. 80 with permission from Springer Nature, copyright © 2020.

Table 1 Spin density distribution of condensed-phase triplet ground-state metallonitrenes and arylnitrenes

	Spin density distribution				
Compound	$N_{nitrene}$	$Ring_{central}$	Metal	Level of theory	Ref.
35	1.81*e*	—	0.13*e*	PBE0/def2-TZVPP	80
37	1.92*e*	—	0.07*e*	PBE0/def2-TZVPP	81
46	1.41*e*	0.52*e*	—	B3LYP/6-311+G(2df, p)	82
48[a]	1.53*e*	0.29*e*	—	B3LYP/def2-SVP	83

[a] For nitrene **48**, a truncated model was employed in which the alkyl substituents on the supporting ligand (M^{S}Fluind*) were replaced by hydrogen atoms.

reaching a plateau at temperatures below 50 K (**35**) and 20 K (**37**). Beyond 170 K and 210 K, the magnetic moment exhibits a steep decline for complex **35** and an increase for complex **37**, which could be attributed to the thermal instability of the metallonitrenes. Notably, ZFS spin-Hamiltonian formalism for the triplet states of metallonitrenes ^{3}**35** and ^{3}**37** modelled the magnetic data with an isotropic g factor (g_{iso} = 2), affording axial ZFS parameters (D = 85 cm^{-1} (**35**) and 9.3 cm^{-1} (**37**)), in good agreement with computed values (D = 73 cm^{-1} (**35**) and 8 cm^{-1} (**37**)) (Table 2). Due to pronounced spin–orbit coupling, both metallonitrenes show no detectable X-band EPR signals. However, the microstate splitting is significantly smaller compared to that of the isoelectronic complexes [Ir(N^{t}Bu)(PNP)] (D = 466 cm^{-1}) and (IrO(PNP)) (D = 647 cm^{-1}), suggesting

Table 2 Comparison of selected spectroscopic parameters of condensed-phase nitrenes discussed in this article

Compound	Spin state	EPR activity	g_{iso}	ZFS (D)/cm^{-1}	E/D
Phosphinonitrene (**29**)[7]	Singlet	Inactive	—	—	—
[Pt(N)(PNP)] (**35**)[80]	Triplet	Inactive	2.0[a]	85[a]	0.08[a]
[Pd(N)(PNP)] (**37**)[81]	Triplet	Inactive	2.0[a]	9.3[a]	0.11[a]
M^{S}FluindN (**46**)[82]	Triplet	Active	2.00145[b]	—	—
M^{S}Fluind*N (**48**)[83]	Triplet	Active	2.00	0.879[c]	0.002[c]

[a] Obtained from simulation of SQUID magnetometric data. [b] Obtained from an EPR spectrum recorded in benzene solution at room temperature. [c] The data presented in this report were obtained from the *Heron 10 Conference on Reactive Intermediates and Unusual Molecules*, held from 6 to 12 July **2025** in Australia, as reported by the lead author of the referenced study.

reduced effective spin–orbit coupling. Quantum-chemical calculations demonstrated that metallonitrenes exhibit triplet ground states with substantial singlet–triplet energy gaps ($\Delta E_{S\rightarrow T}$ = 15 kcal mol^{-1} (**35**) and 18 kcal mol^{-1} (**37**); Fig. 11) and the spin density is localized primarily on the nitrene nitrogen (91% (**35**) and 96% (**37**)). The characteristic NLMOs resulting from NBO analysis of the ground-state wave function at the PBE0/def2-TZVPP level of theory indicate, for both metallonitrenes **35** and **37**, the presence of an M–N σ-bond, a lone pair, two singly occupied p orbitals at the nitrogen, and four non-bonding metal d-orbitals (Fig. 4).[80,81]

Pt metallonitrene **35** exhibits ambiphilic reactivity. Consistent with the subvalent structure of a metallonitrene, **35** participates in a variety of NAT reactions as an electrophile, reacting with CO and PMe_3 to generate the corresponding isocyanate **38** and phosphoraneiminato complex **39**, respectively. Complex **35** also reacts with various electrophilic reagents: **35** reacts with aldehydic C–H bonds of benzaldehyde and 1-butanal, B–H bonds of HBPin, and B–C bonds of BPh_3 to generate the corresponding Pt(II) amido complexes **40–43**, as illustrated in Scheme 7.

Hammett's analysis of the reaction of metallonitrene **35** with substituted benzaldehydes, carried out under steady-state photolysis, was consistent with a rate-determining nucleophilic attack of the metallonitrene on the aldehyde. Moreover, notwithstanding the subvalent nitrene character inherent in metallonitrene **37**, the selective C–H insertion with aldehyde proceeds *via* a nucleophilic-driven pathway. The transamidation of the resultant benzamide product is subsequently facilitated through its reaction with Me_3SiN_3 (Scheme 8).

2.2.3. Triplet ground-state organic nitrenes. The isolation and characterization of singlet ground-state organic nitrenes in the condensed phase were achieved a decade ago; however, the isolation of triplet ground-state arylnitrenes remains a significant challenge. Quantum-chemical calculations suggested that while the π-donating ligands coordinated to the nitrene atom ($N_{nitrene}$) stabilize the singlet ground state, σ-donating ligands favour the triplet ground state.[5,6] In 2024, the Beckmann and Tan groups independently and concurrently reported the successful isolation of triplet ground-state arylnitrenes, whose remarkable stability arises from the kinetic shielding by a hydrindacene ligand.[82,83] This class of ligands, originally introduced by Matsuo, Tamao, and coworkers, is designed to maximise the steric bulk and minimize rotational freedom.[84] This efficiency is attributed to a well-protected pocket within the ligand framework, which provides a protec-

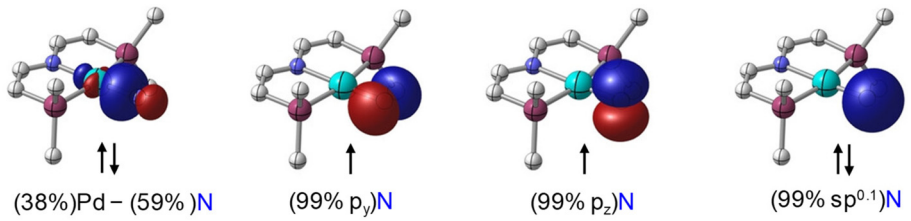

Fig. 4 Characteristic NLMOs resulting from NBO analysis at the PBE0/def2-TZVPP level of theory for **37**.[81]

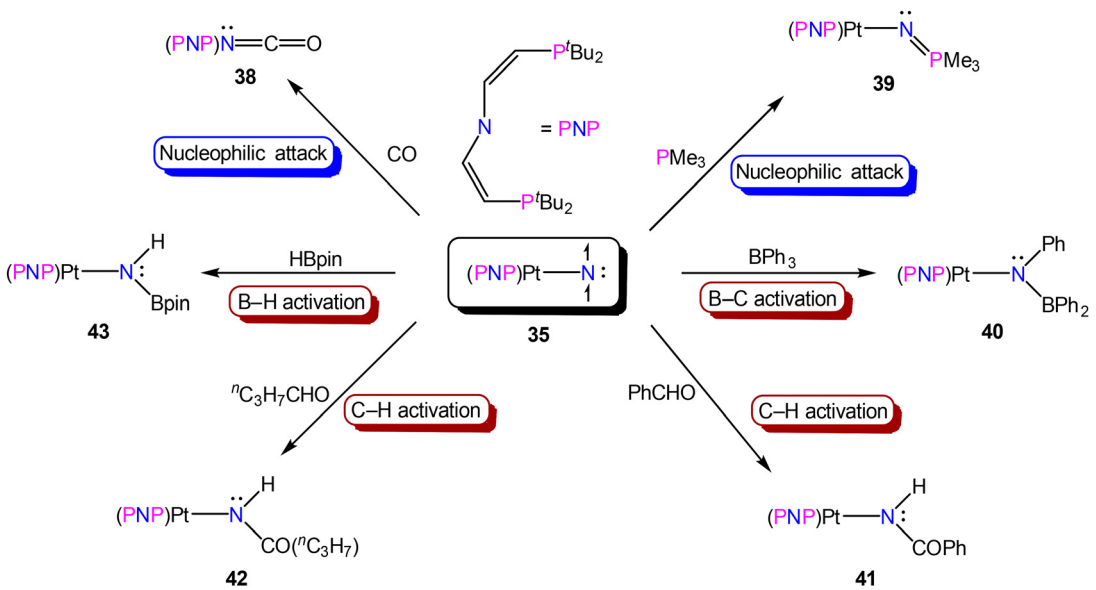

Scheme 7 Nitrogen-centered reactivity of metallonitrene **35**.[80]

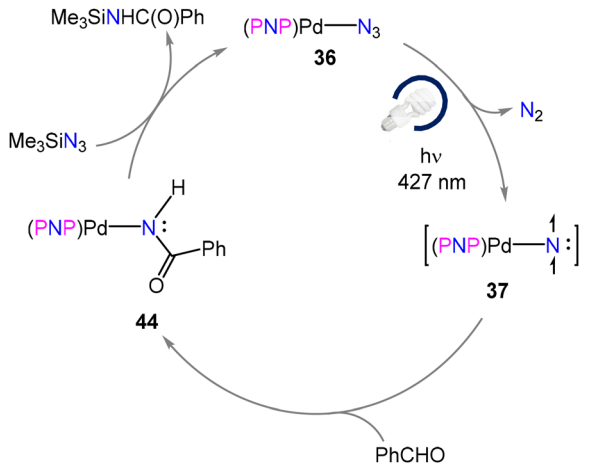

Scheme 8 Proposed catalytic cycle for C–H insertion and transamidation.[81]

tive environment to stabilize main-group centers.[84–90] Irradiation of the aryl azides M^SFluindN$_3$ (**45**) and M^SFluind*N$_3$ (**47**) (where M^SFluind & M^SFluind* are hydrindacene-based ligands) affords the corresponding triplet ground-state arylnitrenes **46** (Beckmann and coworkers) and **48** (Tan and coworkers), respectively (Scheme 9). Arylnitrenes **46** and **48** were comprehensively characterised *via* sc-XRD and EPR spectroscopy. Spectroscopic analyses unequivocally confirmed that compounds **46** and **48** possess triplet ground-state electronic configurations.

sc-XRD analyses of arylnitrenes **46** and **48** revealed that both possess nearly identical core skeletal arrangements and bonding metrics. In nitrenes **46** and **48** (Fig. 5a),[83] C^{ipso}–$N_{nitrene}$ lengths (1.327(2) Å (**46**) and 1.317(3) Å (**48**)) are considerably shorter than those observed in the corresponding primary amines M^SFluind/M^SFluind*–NH$_2$ (1.382(2) Å (**46**) and 1.394(2) Å (**48**)),[83] diminishing any possibility of the presence of an N–H moiety. However, these bond lengths slightly exceed the C=N double-bond length observed in diaminobenzoquinoneimine (1.293 Å),[91] showing their double-bond character. Interestingly, both nitrenes **46** and **48** exhibit significant bond-length variations in the core phenyl ring compared to the corresponding primary amines M^SFluind/M^SFluind*–NH$_2$. This difference, which reflects the disparity in the average lengths of longitudinal C–C bonds relative to the transverse bonds along the C–N bond axis, suggests a quinoidal electronic structure due to the delocalization of the unpaired electron (Fig. 5a).

The high-spin ground state for solid samples of **46** was established using a SQUID magnetometer. For nitrene **48**, Tan and coworkers used solid-state EPR, SQUID measurements, and solution-phase Evans' nuclear magnetic resonance spectroscopy. As expected for $S > 1/2$ spin systems, Tan and coworkers showed that **48** is EPR-silent at room temperature due to fast relaxation. They observed an isotropic signal centred at $g = 2.0$, which was assigned to an impurity with a doublet spin state. Beckmann and coworkers also observed a similar signal, and they interpreted it as an indication of spin delocalization within the aryl ring in sight of hyperfine coupling (A_H = 17 MHz) with the p-hydrogen. The EPR spectrum of **48** was measured at cryogenic temperatures. It revealed a principal signal at 670 mT, assigned to the transition in the *xy*-plane of the *D*-tensor, as well as a signal at 195 mT assigned to the triplet transition between the $M_s = \pm 1$ magnetic sublevels. Nitrene **48** shows substantial axial zero-field splitting (D = 0.92 cm^{-1}) in the standard range of aryl-substituted triplet nitrenes with vanishing rhombicity (E/D = 0.002) (Table 2), thereby confirming that the two unpaired electrons are at least partially localized at the nitrogen atom (Table 1). DFT calculations also demonstrated that over two-thirds of the total spin resides on the nitrene nitrogen atom. This observation suggests that the two resonance structures, which relate to either the triplet nitrene or the iminyl radical, have approximately equal contributions (Fig. 5b).

Tan and coworkers also studied the intermolecular activation of small molecules by triplet nitrene **48**. Although pre-

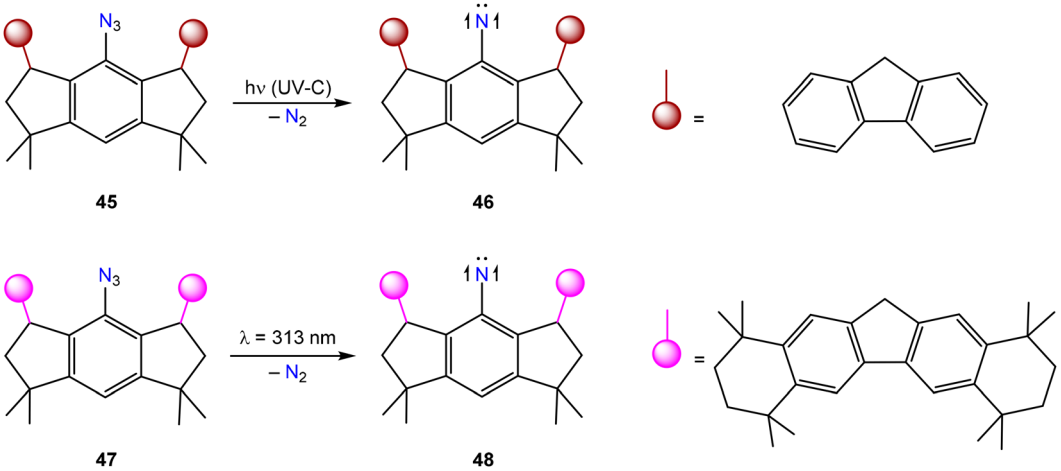

Scheme 9 Synthesis of room temperature stable triplet ground-state arylnitrenes **46** and **48**.[82,83]

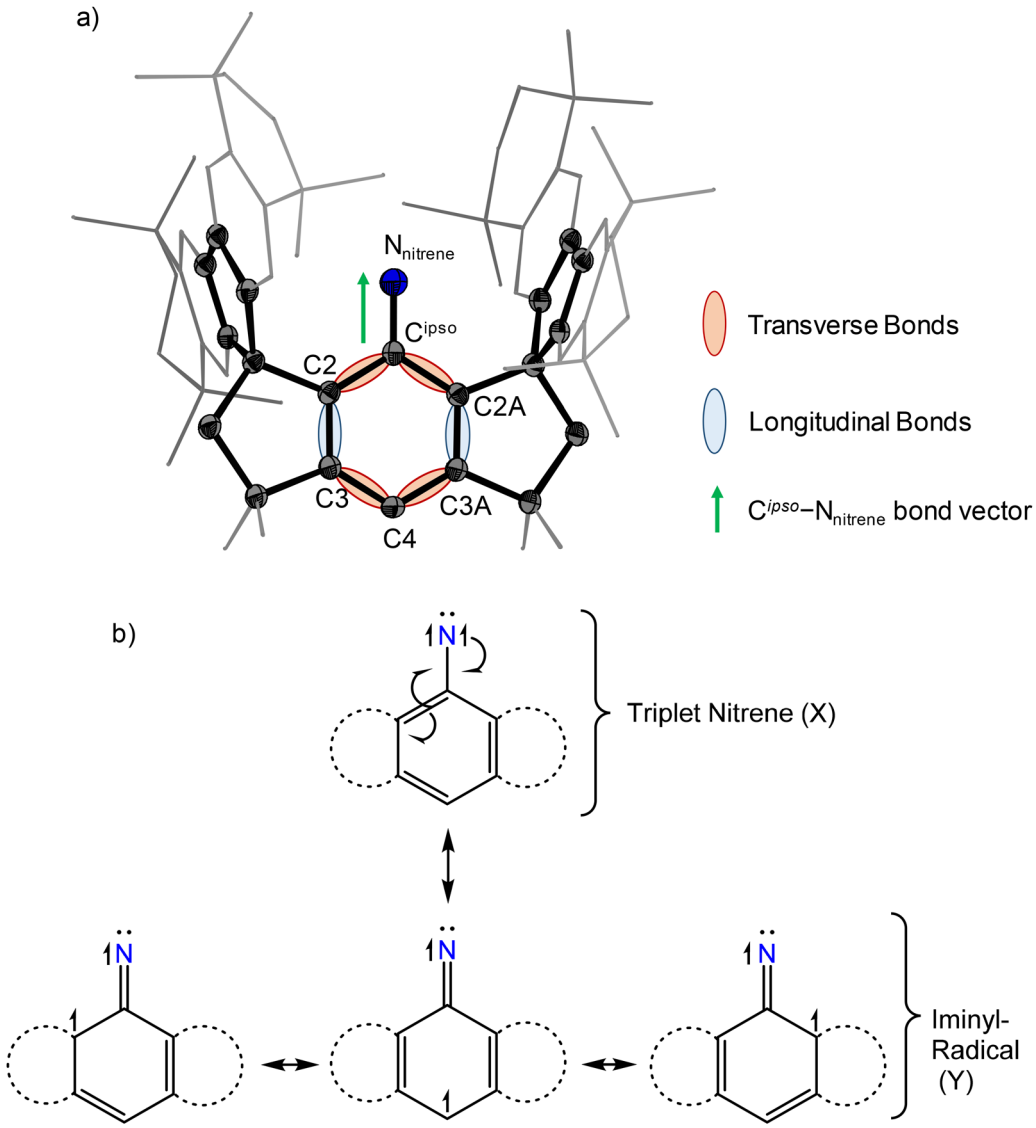

Fig. 5 (a) Molecular structure of triplet ground-state arylnitrene **48**, reproduced from ref. 83 with permission from Springer Nature, copyright © 2024. (b) Resonance structures for **46** and **48**, illustrating the superposition of the two dominant contributing forms: the nitrene (X) and the iminyl radical-based (Y) resonance structures.

liminary in nature, their experimental observations suggest remarkable chemical stability, in line with the persistence reported for **46** in CH_2Cl_2. For comparison, isolated late transition metal-supported nitrenes react instantaneously with weak H-atom donors; in some cases, handling these compounds requires silanized glassware to prevent H-atom abstraction from the glass surface.[78,92] However, nitrene **48** is relatively stable in THF. The H-abstraction reaction to form the corresponding primary amine (**50**) requires 9 hours at room temperature. Likewise, the C–H insertion reaction with a large excess of DMF requires about 3 hours to afford secondary amine **51**, while aziridination of styrene (**52**), and the formation of the iminophosphorane **49** upon reaction with PMe_3 require 5 and 6 hours, respectively (Scheme 10).[83]

3. "Bottleable" base-/metal-free pnictinidenes

3.1. Phosphinidenes

Phosphinidenes are heavy congeners of nitrenes that have been broadly used as *in situ* reagents in synthetic phosphorus chemistry and also serve as versatile ligands in coordination with transition metals.[93–99] Although the parent phosphinidene is commonly found in interstellar clouds and the atmospheres of distant planets, the substantial reactivity of phosphinidenes has made their isolation particularly challenging.[100] The parent phosphinidene (HP) exhibits a triplet ground state, which is estimated to be approximately 20–28 kcal mol^{-1} more

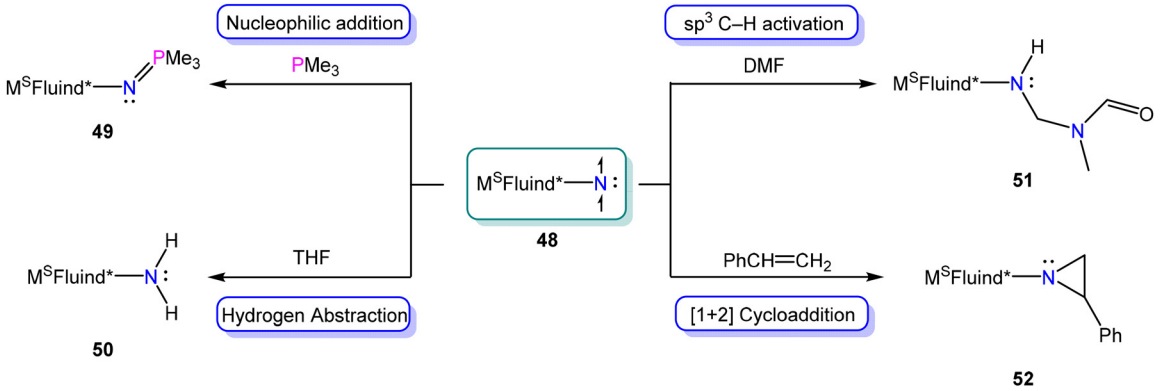

Scheme 10 Reactivity studies of triplet ground-state arylnitrene **48**.[83]

stable than its singlet state.[101] The stability difference is significantly greater than that observed for the parent carbene CH_2, where the triplet state is favoured by only about 9 kcal mol^{-1}.[102] The energy difference between the singlet and triplet states ($\Delta E_{S\rightarrow T}$) of phosphinidenes is highly influenced by the electronic properties of their substituents. Transient phosphinidenes react with various NHCs to form stable NHCPs. The rapid development of NHCPs has been comprehensively reviewed in a recent article by Inoue and coworkers.[103] The concept article by Zeng and coworkers provides a concise review of recent experimental advances in the preparation, characterization, and reactions of prototypical phosphinidenes.[104] Although numerous examples of base-supported phosphinidenes[105] are well documented in the review article by Dostál and coworkers,[4] their structures are often perturbed due to the electron-density donation from the particular Lewis base to the electron-deficient phosphorus centre. In a broader view, various NHCs form stable adducts with transient phosphinidenes to afford NHCPs and are widely used to stabilize low-coordinate main-group elements. In this work, we present a chronological account of the detailed studies on base- and metal-free condensed-phase singlet and triplet ground-state phosphinidenes.

3.1.1. Stable singlet phosphinidene. The parent phosphinidene (HP) has a triplet ground state. It has a considerable singlet–triplet energy separation, underscoring the inherent challenge associated with isolating phosphinidene derivatives with a singlet ground state. As previously mentioned, strong π-donor substituents or ligands are expected to stabilize elusive nitrenes and heavier pnictinidenes in their singlet ground state. By employing this strategy, a stable (phosphino) phosphinidene was successfully isolated using a synthetic route that involved the evolution of CO from the corresponding (phosphino)phosphaketene (**54**) (Scheme 11) by Bertrand and coworkers in 2015.[106] The phosphinidene center is coordinated to a 1,3,2-diazaphospholidene framework, deliberately selected as a supporting ligand.[5] However, it necessitates shielding with highly sterically demanding protecting groups; without such protection, it readily undergoes dimerization, resulting in the formation of a diphosphene (RP═PR). As expected for a singlet ground-state phosphinidene, **55** features a high degree of multiple-bond character between the two phosphorus centers, as shown by the resonance forms **55b** and **55c**. This is reflected in the very short P–P bond length (calcd. 1.917 Å) and the large phosphorus–phosphorus coupling constant (^1J(P,P) = 884 Hz). However, direct evidence for the molecular structure of (phosphino)phosphinidene **55** *via* sc-XRD is currently unavailable.

NBO analysis, performed at the M06-2X/def2-TZVPP//M06-2X/def2-SVP level of theory on a truncated model of compound **55** (where the Dipp group was replaced by Ar), yielded a WBI of 2.34 for the P–P bond, suggesting considerable double-bond character. The canonical molecular orbitals of (phosphino) phosphinidene **55** reveal that the HOMO and HOMO−1 corres-

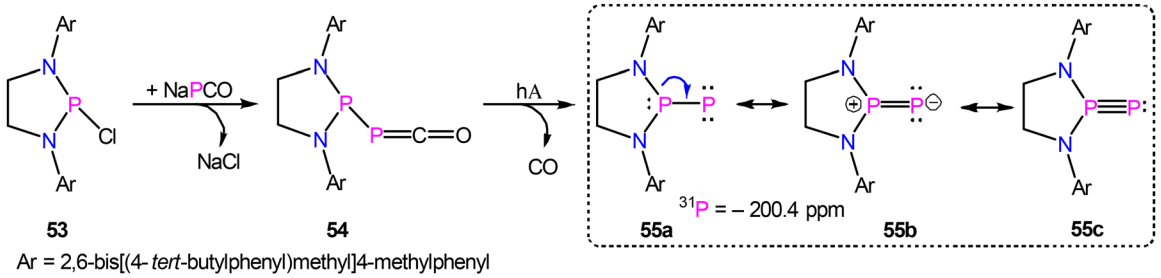

Scheme 11 Synthesis of the singlet ground-state (phosphino)phosphinidene **55**.[106]

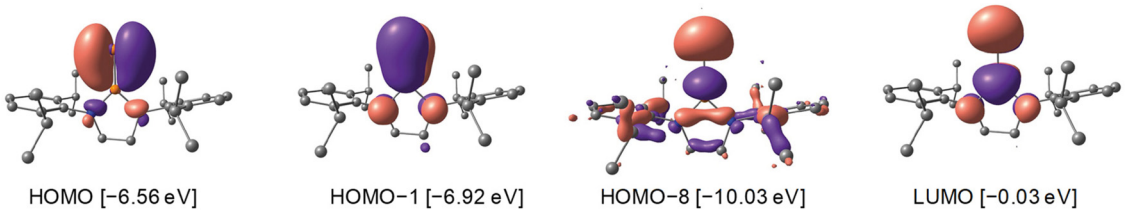

Fig. 6 Selected frontier molecular orbitals of **55**, calculated at the M06-2X/def2-TZVPP//M06-2X/def2-SVP level of theory, adapted from ref. 106 with permission from Elsevier, copyright © 2016 Elsevier Inc.

pond to the in-plane and out-of-plane terminal phosphorus-centered P–P π orbitals, respectively. The HOMO−8 represents the P–P σ-bonding orbital, while the LUMO is identified as the P–P π-antibonding orbital (Fig. 6).

NPA indicates that the terminal P is negatively charged (−0.34 au), whereas the endocyclic P carries a large positive charge (+1.16 au). Based on these results, similar to singlet carbenes and nitrenes, singlet phosphinidene **55** is expected to be predominantly nucleophilic. Notably, the coordination of CO to the phosphinidene center to afford phosphaketene **54** exhibits reversibility, showcasing a reactivity pattern reminiscent of transition metals. It readily engages in [1 + 2] cycloaddition reactions with electron-deficient alkenes or exhibits addition reactions with isocyanides, yielding the cycloaddition products **57** and the addition products **60**, respectively. Additionally, Bertrand and coworkers have shown experimental evidence that despite its P–P multiple bond character and the presence of a negative charge on the phosphinidene center, **55** acts as an electrophile by reacting with strong σ-donor and weak π-acceptor ligands (phosphanes and N-heterocyclic carbenes) to afford the corresponding Lewis acid–base adducts **57** and **58**, respectively (Scheme 12).[107]

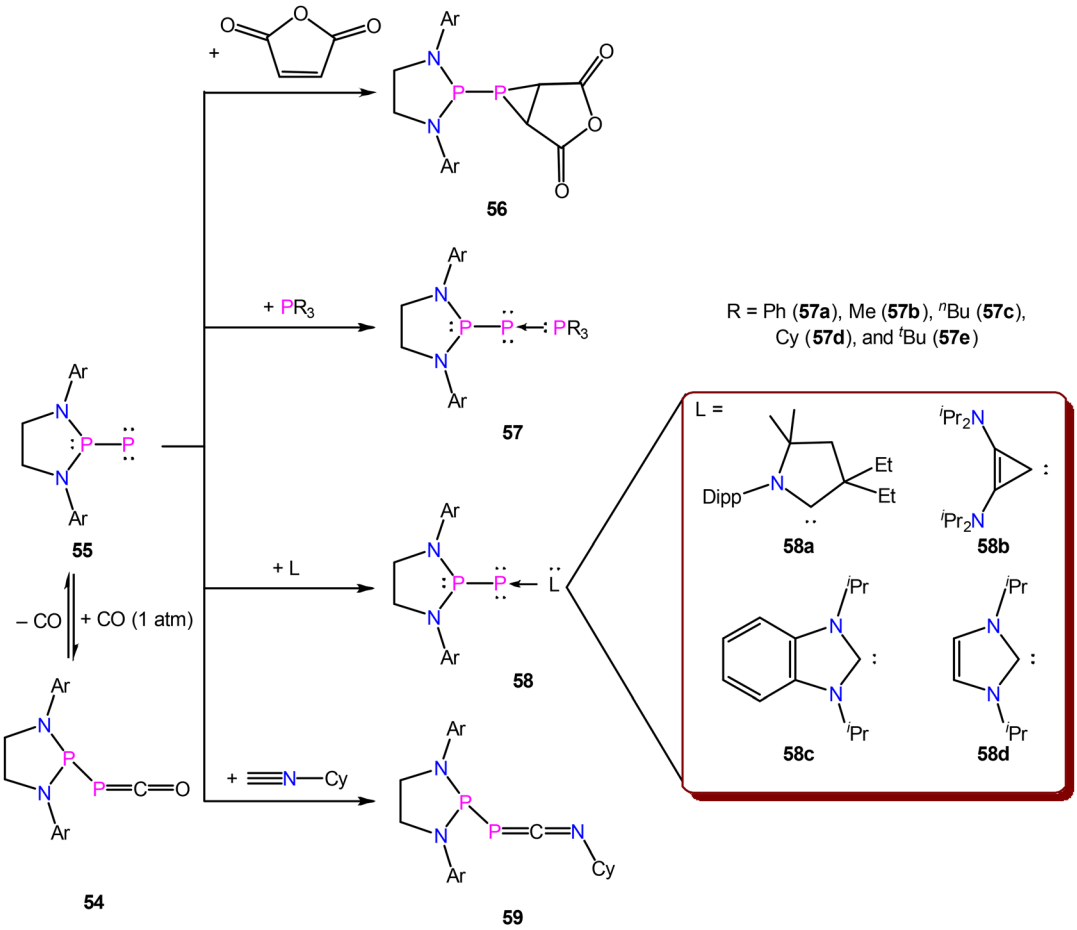

Scheme 12 Reactivity of singlet (phosphino)phosphinidene **55**.[107]

3.1.2. Molecular-strain-induced phosphinidenes: phosphanorcaradienes. Tan and coworkers attempted to isolate a stable, triplet ground-state phosphinidene supported by a hydrindacene ligand by dehalogenating the corresponding phosphorus(III) dichloride $M^{S}Fluind^{tBu}$-PCl_2 (**60**) with two equivalents of KC_8 in THF. However, the expected monocoordinated phosphinidene (**62**) was not detected; instead, phosphanorcaradienes (**61**) were isolated as a yellow solid in 75% yield.[108] Phosphanorcaradienes, the phosphorus analogues of norcaradienes (NCDs),[109,110] are an appealing class of phosphorus compounds that can serve as synthons for phosphinidenes. The presented phosphanorcaradiene (**61**) revealed that one of the benzene rings in the flanking fluorenyl moieties is intramolecularly dearomatized upon attachment to the phosphorus center. The formation of the PC_2 three-membered ring in **61** leads to a decrease in the symmetry and complex ^1H and $^{13}C\{^1H\}$ NMR spectra. sc-XRD analysis unambiguously confirmed the dearomatization of the flanking fluorenyl motif and the formation of a strained PC_2-ring. The molecular structure of **61** revealed that the phosphorus atom and the activated carbons of the benzene ring of the flanking fluorenyl motif are connected *via* stretched P–C single bonds ($P–C^{activ1}$ = 1.973(5) Å, $P–C^{activ2}$ = 1.985(5) Å), consequently leading to a more acute angle at the P center ($C^{activ1}–P–C^{activ2}$ = 43.78(19)°). Additionally, the phosphorus center is considerably deviated from the position expected for an atom attached to a phenyl group, suggesting increased ring strain in the PC_2 ring of **61** compared to typical phosphiranes. Quantum-chemical calculations on **61** at the BP86 + D3Bj/def2-SVP level of theory also confirmed the stretched, weak bonds between phosphorus and the activated carbons of the benzene motif, as evidenced by WBIs of 0.74 ($P–C^{activ1}$) and 0.72 ($P–C^{activ2}$). Furthermore, compound **61** is more stable by approximately 5.7 kcal mol^{-1} energy compared to the anticipated free phosphinidene **62** (Fig. 7).[108]

Interestingly, **61** shows thermal stability but acts as a synthetic equivalent of the anticipated free phosphinidene. For instance, **61** undergoes Lewis acid–base adduct formation with PMe_3 and isocyanide (XylNC) to afford phosphanylidene–phosphorane **63** and 1-phospha-3-azaallenes **64**, respectively. It also shows single-fold and double-fold addition reactions with arylazide (RN_3, R = 4-^{t}Bu-C_6H_4) to afford stable iminophosphane **65** and bis(imino)phosphanes **66**, respectively. Moreover, **61** is capable of activating ethylene and terminal alkynes in a formal [1 + 2] cycloaddition manner to afford the corresponding cycloaddition products (**67** and **68**, respectively). **61** also demonstrates oxidative cleavage of polar Si–H and N–H bonds to yield secondary phosphines **69** and **70**, respectively (Scheme 13).[108]

3.2. Arsinidenes

In 1996, Weber and coworkers reported the synthesis of compound $(Me_3Si)AsC(NMe_2)_2$ (**73**),[111] achieved by a salt metathesis reaction between the metalloarsaalkene thiuronium salt

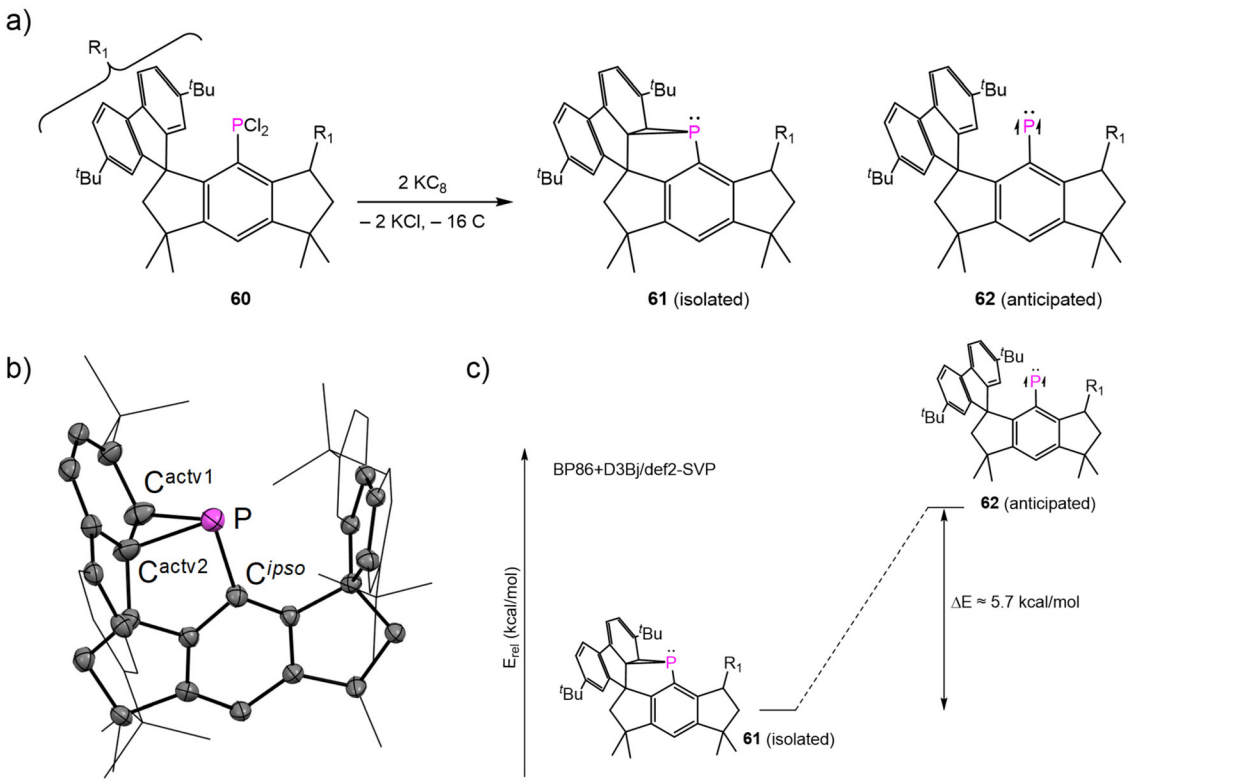

Fig. 7 (a) Synthesis of phosphanorcaradiene **61**. (b) Molecular structure of **61**. (c) Graphical representation of the calculated energy separation between the energy minimum **61** and the anticipated triplet ground-state phosphinidene **62**.[108]

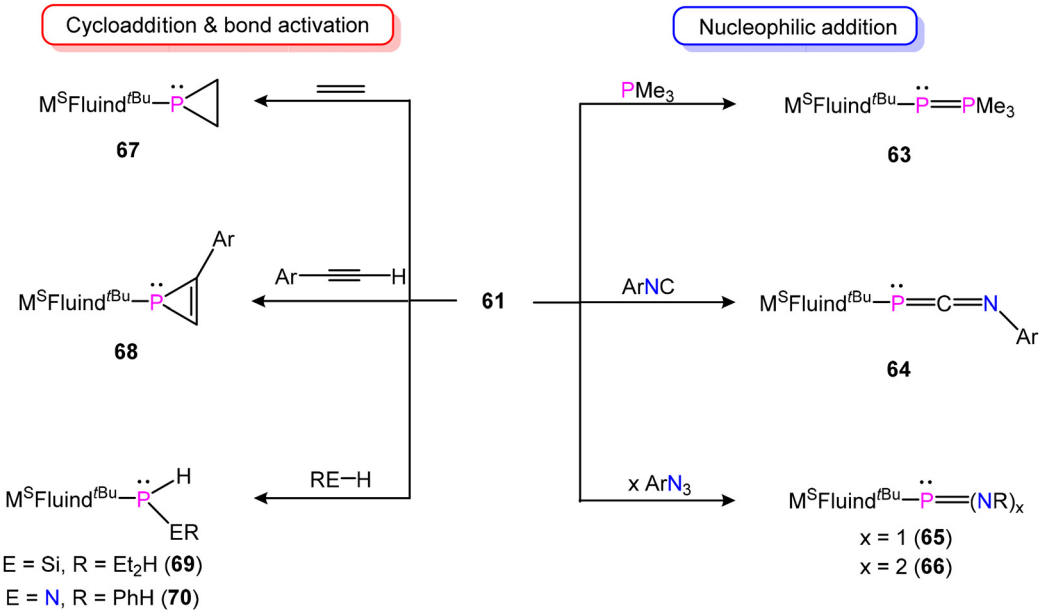

Scheme 13 Reactivity of phosphanorcaradiene **61** demonstrates its potential as a masked triplet ground-state phosphinidene.[108]

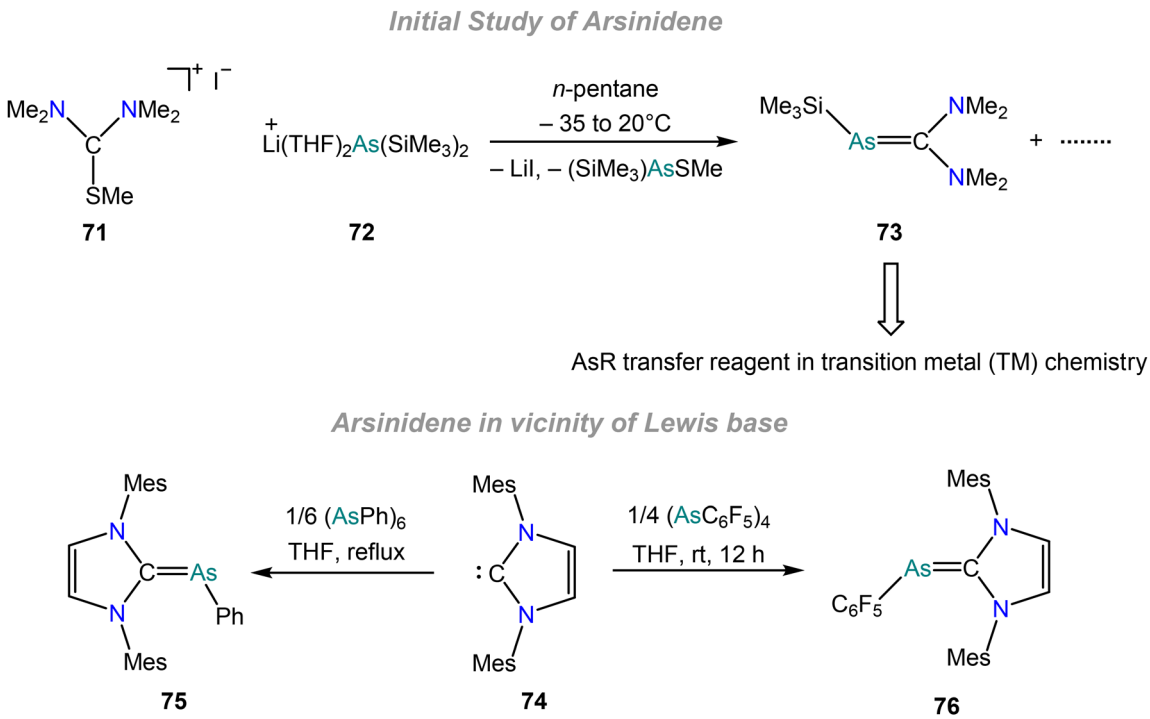

Scheme 14 Isolation of inversely polarized arsaalkenes, which are used as arsinidene-transfer reagents in TM chemistry, and a few examples of structurally characterized arsinidenes in the vicinity of Arduengo's NHC.[111,113]

$[(Me_2N)_2CSMe]I$ (**71**) and an equimolar amount of the lithiated salt $Li(THF)_2{\cdot}As(SiMe_3)_2$ (**72**) (Scheme 14). Notably, due to the oily nature of **73**, no sc-XRD structure was obtained. Subsequent reactivity studies revealed its role as an arsinidene-transfer reagent.[112] Subsequently, Lewis base-supported and structurally characterized arsinidenes were reported by Arduengo and coworkers, who achieved this by the disintegration of cyclic oligomers $(RAs)_x$ (R = Ph (**75**; x = 6), C_6F_5 (**76**; x = 5)) through the use of NHC (**74**) (Scheme 14).[113] Following this, several intermolecular and intramolecular base-supported arsinidenes have been thoroughly characterized at the structural level and subjected to comprehensive, in-depth

studies.[37,114–119] The isolation of arsinidenes in their monomeric state proves to be an uphill task owing to their inherent tendency to undergo dimerization or oligomerization, leading to the formation of higher-order species. Nevertheless, base- and metal-free arsinidenes, whether in their singlet or triplet ground state, remain structurally uncharacterized to date, posing a significant challenge for future investigation.

3.3. Stibinidenes

In 2010, Dostál and coworkers demonstrated that the combination of steric shielding and intramolecular Sb···N interactions, which protect both the empty p-type and the lone p-type orbitals of the central Sb atom, facilitated the isolation of the first monomeric stibinidene featuring a NCN 2,6-bis(ketimine)/bis(aldimine)phenyl pincer ligand.[37,120] Structural investigations of Dostál's bis(aldimine) and bis(ketimine)-based NCN-pincer ligand system revealed that both N atoms are involved in the coordination of the Sb atom, giving rise to hypervalent bonding. Recently, Beckmann and coworkers isolated a series of arylpnictinidenes 2,6-$(Ph_2PNMes)_2C_6H_3Pn$ (Pn = As, Sb, Bi) based on a novel bis(phosphine imine) NCN-pincer ligand and studied their oxidation chemistry with chalcogens (Ch = S, Se, and Te), affording arylpnictinidene chalcogenides possessing a heavily polarized $^{+}$Pn–Ch^{-} single bond.[121] Nevertheless, stibinidenes have also been explored in the vicinity of Lewis bases[40,122] and transition metal complexes.[123–129] However, the isolation of a truly monocoordinated stibinidene has remained elusive, presenting significant challenges for experimental chemists. Tan and coworkers reported the successful isolation and detailed characterization of the unprecedented triplet state, base-free stibinidene M^{S}Fluind*–Sb (M^{S}Fluind* = hydrindacene ligand).[130] Commercially available SbX_3 (X = Cl, Br) undergoes salt metathesis with lithiated hydrindacene M^{S}Fluind/M^{S}Fluind$^{tBu/}$*Li$(thf)_2$ (Scheme 15) to afford colorless crystalline complexes M^{S}Fluind/M^{S}Fluind$^{tBu/}$*–SbX_2 (X = Cl, Br) (**77a–d**) under ambient conditions. Cornella and coworkers also reported the dehalogenation of M^{S}Fluind^{tBu}/M^{S}Fluind–SbX_2 (**77c** and **77d**) using decamethylcobaltocene (Cp^*_2Co) as a reducing agent, resulting in the corresponding distibenes **78b** and **78c** as the only products.[131] Dehalogenation of Tan's M^{S}Fluind$^{tBu/}$*–SbX_2 with two equivalents of KC_8 or Jones' Mg dimer[132] yielded distinct products: distibene **78a**, isolated as a purple crystalline solid, and stibinidene **79**, obtained as yellow crystals (Scheme 15). Notably, the steric bulk of the flanking fluorenyl substituents plays a crucial role in determining the nature of the resulting product.

The ^{1}H and ^{13}C{^{1}H} NMR spectra of compound **79**, measured in (D_6)benzene at 298 K, exhibit paramagnetic chemical shifts in the ranges δ_H = −82.34 to 14.46 ppm and δ_C = −236.7 to 277.3 ppm. The infrared spectrum of stibinidene **79** reveals an absence of peaks within the 1850–2000 cm^{-1} range, a characteristic region for the stretching vibration of Sb–H bonds.[133] This observation strongly indicates the

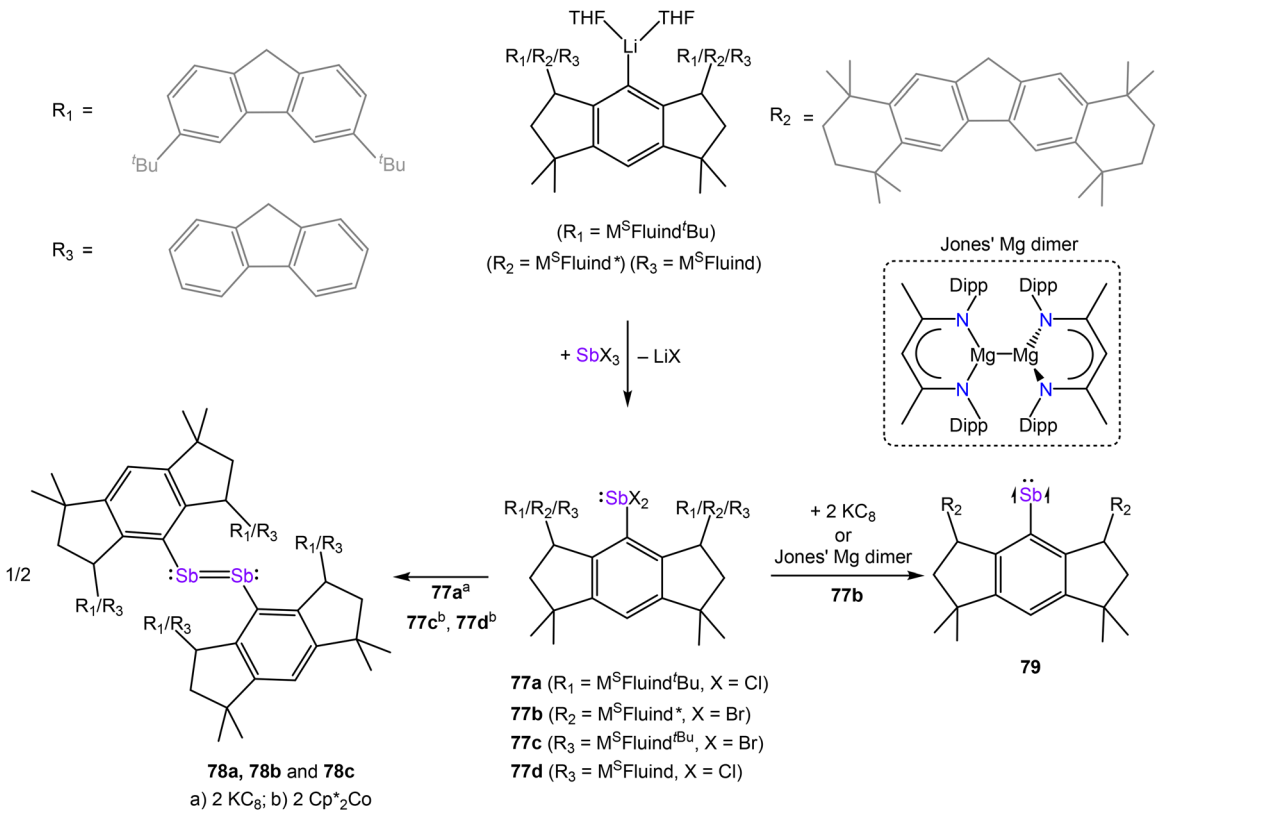

Scheme 15 Dehalogenation of M^{S}Fluind/M^{S}Fluind$^{tBu/}$*–SbX_2 (X = Cl, Br) to afford distibenes **78a–c**[131] and triplet-state stibinidene **79**.[130]

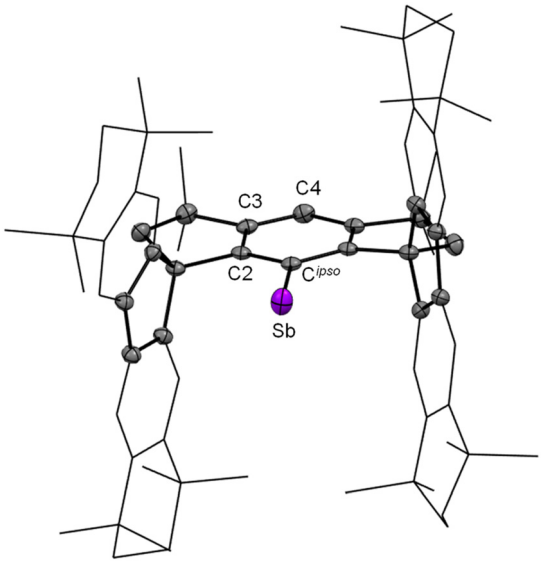

Fig. 8 Molecular structure of triplet-state stibinidene **79**, reproduced from ref. 130 with permission from Elsevier, copyright © 2023 Elsevier Inc.

absence of any hydrogen atoms bonded to the Sb center. X-ray crystallographic characterization of **79** (Fig. 8),[130] crystallizing in the monoclinic space group *C*2/*c* and exhibiting *pseudo*-C_{2v} symmetry, showed a one-coordinated Sb center bound to the central phenyl ring of the hydrindacene ligand with an Sb–C^{ipso} bond length of 2.143(6) Å. This value aligns closely with the Sb–C^{ipso} single-bond length observed in distibene $(Ar^{Mes}Sb)_2$ (2.169(4) Å).[26] The extended Sb center to carbon atom distance (3.241(2) Å) within the flanking fluorenyl moieties underlines solely non-covalent interaction between the Sb and C atoms ($\Sigma d(Sb–C)_{covalent}$ radii = 2.15 Å, $\Sigma d(Sb–C)_{van\ der\ Waals}$ radii = 3.76 Å). NCI[134] analyses conducted *via* DFT calculations reveal that the interaction between the Sb center and the flanking fluorenyl moieties predominantly arises from dispersion forces.[130]

Despite a triplet ground-state configuration, Tan's stibinidene **79** exhibits no observable signal in its EPR spectrum. However, the effective magnetic moment (μ_{eff}) of stibinidene **79**, determined *via* Evans' method at 293 K, was found to be 1.96μ_B, a value that aligns well with its paramagnetic character.[130] Additionally, the temperature dependence of the magnetic susceptibility–temperature product ($\chi \cdot T$), measured *via* SQUID magnetometry, shows a linear dependence on temperature and remains unsaturated even at 300 K. This behaviour is in excellent agreement with the presence of a triplet ground state for stibinidene **79**. Consequently, stibinidene **79** is confirmed to possess a triplet ground state, although the magnetic properties deviate significantly from those typically observed for S = 1 spin-state complexes. This irregular behaviour could be attributed to a large ZFS (D = 940 cm^{-1} obtained from quantum chemical calculations),[130] which leads to an energetically isolated M_S = 0 ground state. It is well established that the magnetic characterization of triplet states exhibiting ZFS exceeding 1000 cm^{-1} presents formidable technical challenges. Fixed-frequency EPR is typically the preferred technique for accurate determination of ZFS within the GHz range; however, it becomes ineffective when the energy separation between the M_S levels, induced by ZFS, exceeds the excitation energy of the spectrometer (10 GHz or 0.3 cm^{-1} for a standard X-band EPR spectrometer).[135] This phenomenon explains the EPR inactivity of triplet ground-state stibinidene **79**, as the large ZFS places the energy gap between the M_S levels beyond the excitation capability of standard X-band EPR spectrometers. A computational analysis using CASSCF/NEVPT2 was performed on a model compound $\mathbf{79_{model}}$ (replacing substituents on the supporting ligand with H) and revealed that the triplet ground state of $\mathbf{79_{model}}$ features a leading electronic configuration and is 65.6 kJ mol^{-1} below the lowest-energy S = 0 state (Fig. 11). The nearly degenerate $5p_x$ and $5p_y$ orbitals contribute equally to the total spin population, resulting in a doughnut-like spin density around the Sb centre (spin population = 1.97*e*).[130]

The ambiphilic character of the triplet-state stibinidene **79**[130] is demonstrated by its complexation with the transition-metal Lewis acid $Fe(CO)_4$ fragment to form the stibinidene–iron complex M^SFluind*–Sb → $Fe(CO)_4$ (**80**) and σ-donor Lewis basic N-heterocyclic carbene (IMe_4) to yield the base-supported stibinidene complex **81**. Additionally, stibinidene **79** undergoes cycloaddition reactions with dienes and terminal alkynes, affording Sb-substituted five- and three-membered heterocycles **82** and **83** *via* formal [1 + 4] and [1 + 2] cycloadditions, respectively (Scheme 16). The reactivity of **79** with unsaturated organic compounds resembles that of transient phosphinidenes.[136–138]

3.4. Bismuthinidenes

Bismuthinidenes are a class of organobismuth compounds with the general formula R–Bi. Similar to lighter pnictinidenes, Bi(I) species such as the parent bismuthinidene (BiH) and its methyl derivative (BiMe) are proposed to possess triplet ground states (*vide infra*).[139–141] In the condensed phase, bismuth(I) compounds exhibit a pronounced propensity to undergo dimerization, resulting in the formation of dibismuthenes, or to engage in oligomerization, leading to wider molecular assemblies.[27,142,143] In recent decades, transition metals and polydentate chelating Lewis base ligands, as explored primarily by Dostál and coworkers, have been utilized to stabilize low-valent Bi(I) centers. This stabilization is achieved through steric protection and π-donation, observable in both solution and crystalline structures.[4,37,141] Lewis base-supported bismuthinidenes exhibit a singlet ground state, characterized by an inert lone pair of electrons in the 6*s* orbital.[141] Lichtenberg and coworkers reported the synthesis, spectroscopic characterization, and computational analysis of BiMe, the first non-stabilized bismuthinidene. BiMe was produced through the controlled, stepwise removal of methyl radicals from $BiMe_3$ (**84**) in the gas phase using flash pyrolysis (Scheme 17). Out of three possible structural descriptions of

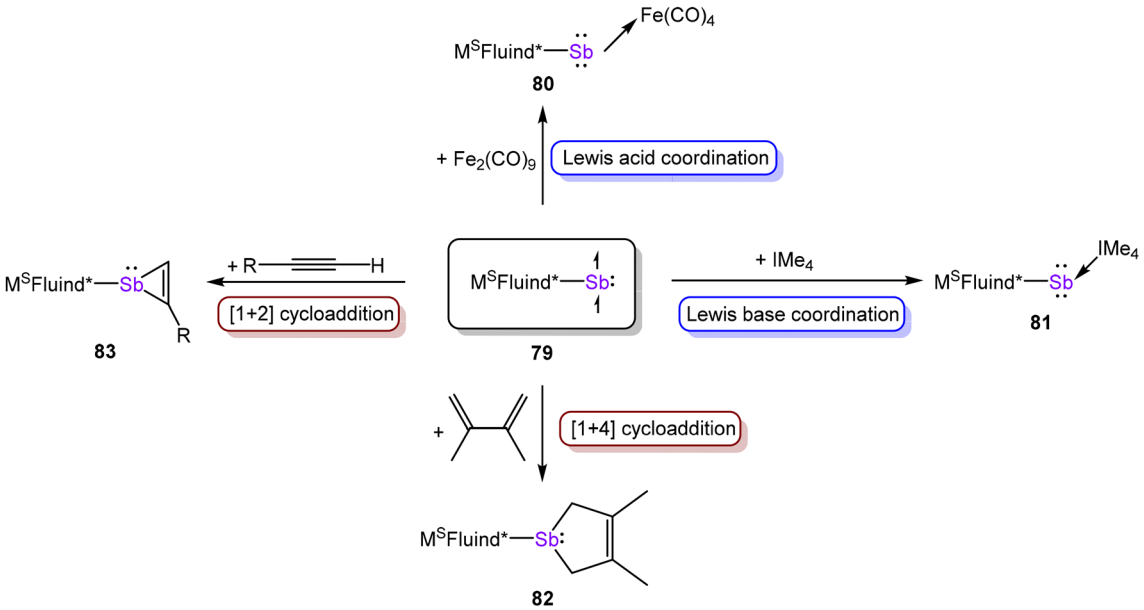

Scheme 16 Reactivity exploration of triplet state stibinidene **79**.[130]

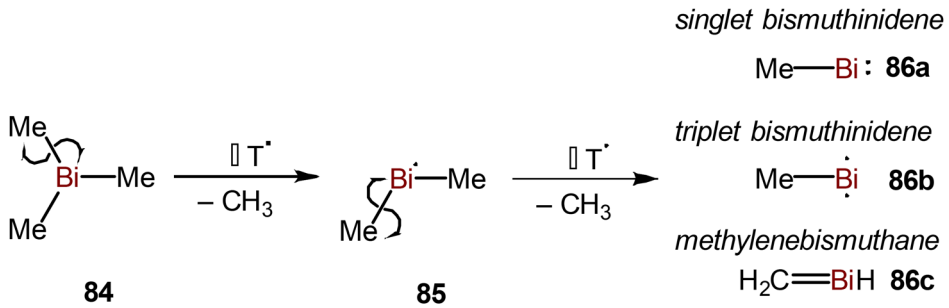

Scheme 17 Generation of the MeBi radical by thermal homolysis of $BiMe_3$ in the gas phase (the $6s^2$ lone pair of electrons is omitted for clarity).[141]

BiMe (**86a–c**), theoretical analysis suggests a triplet (single-center diradical) ground state (**86b**).[141]

In 2023, the groups of Cornella and Tan independently reported the synthesis and condensed-phase characterization of base-free bismuthinidenes possessing triplet ground states, achieved through the strategic employment of sterically demanding hydrindacene ligands.[143,144] The Bi(III) precursors $M^S Fluind^{tBu}$–BiX_2 (X = Cl (**89a**), X = Br (**87**)) and $M^S Fluind^*$–$BiCl_2$ (**89b**) were synthesized *via* salt metathesis between the corresponding lithium salts and BiX_3 (X = Cl, Br) under ambient conditions. Dehalogenation of **87** with the reductant Cp_2Co in toluene under inert conditions afforded the triplet-state bismuthinidene $M^S Fluind^{tBu}$–Bi(I) (**88**) (Scheme 18).[143] Cornella and coworkers reported that dehalogenation of $M^S Fluind$–$BiCl_2$ (**87a**), which contains less sterically demanding substituents, resulted in the efficient synthesis of dibismuthinidene (**88a**) with a high isolated yield. Although bismuthinidene **88** is sensitive to air and moisture, it shows remarkable stability under ambient conditions when stored in an air-free solution or solid state. A THF solution of compound **88** exhibits two relatively weak absorption bands in its UV-Vis–NIR spectrum, located at λ_{max} = 490 nm (visible region) and 1011 nm (near-infrared region). These features suggest the presence of low-energy electronic transitions, which are likely spin-forbidden. Tan and coworkers carried out the 2*e* reduction of Bi(III) compounds **89a** and **89b** using KC_8 under ambient conditions, resulting in the formation of triplet-state bismuthinidenes **90a** and **90b**. These were obtained as yellow crystals in moderate yields (Scheme 18). The absence of Bi–H bonds was confirmed through IR spectroscopy and supported by subsequent reactivity studies (*vide infra*). During the writing of this review article, Schulz and coworkers also reported the synthesis of monocoordinated triplet bismuthinidene. The triplet bismuthinidene Ar*Bi (**92**) stabilized by a very bulky septiphenyl ligand (Ar* = 3,5-^{i}Pr$_2$-2,6-(2,6-Me$_2$-3,5-(2,6-^{i}Pr$_2$C$_6$H$_3$)$_2$-C$_6$H)-C$_6$H) was synthesized by dehydrogenation of *in situ* generated bismuth dihydride Ar*BiH_2 (**91**).[145]

The triplet ground-state bismuthinidenes **88**,[143] **90a**,[144] **90b**[144] and **92**[145] isolated in the condensed phase were characterized using sc-XRD. X-ray diffraction analysis revealed an iso-

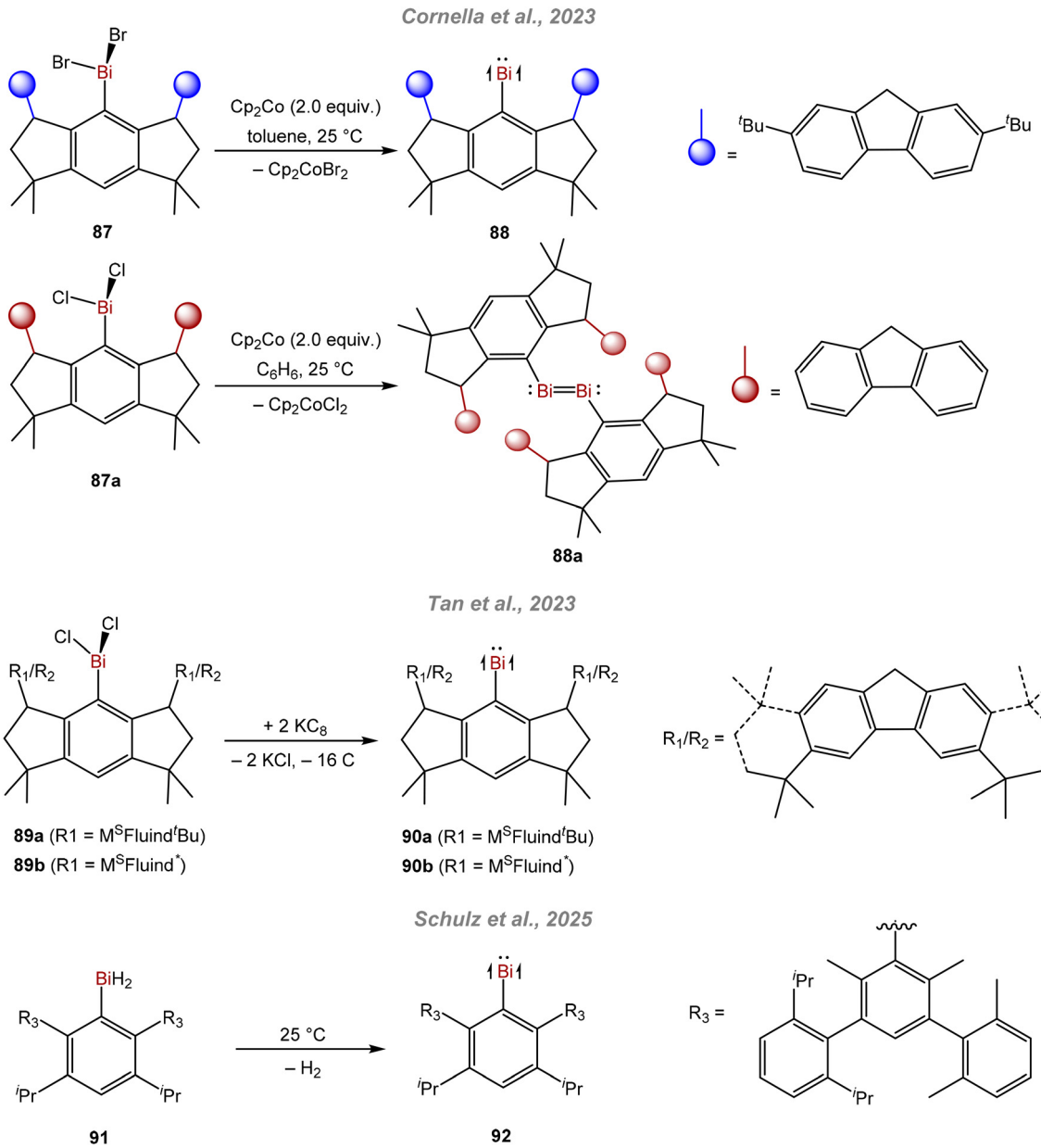

Scheme 18 Synthesis of triplet ground-state bismuthinidenes.[143–145]

typic skeleton arrangement and similar bonding matrices for all four compounds (Fig. 9). For simplicity, only the structural parameters of Cornella's bismuthinidene **88** will be discussed further. The molecular structure of compound **88** supports a monocoordinated bismuthinidene configuration. The shortest Bi···Bi distance in the monomeric structure is 4.385 Å, which exceeds the sum of the Bi···Bi van der Waals radii ($\Sigma d(\mathrm{Bi–Bi})_{\text{van der Waals}}$ radii = 4.14 Å). The Bi–C^{ipso} bond length (2.278(1) Å) indicates a single bond, aligning closely with Pyykkö's single bond radii (2.26 Å).[146] However, it significantly differs from literature-reported *N*,*C*,*N*-pincer bismuthinidenes, where the Bi–C^{ipso} bond distances (2.138(10) to 2.222(5) Å) suggest partial double-bond character.[37,39,147–149] The shortest distance between the central bismuth (Bi) atom and the nearest carbon (C) atom within the adjacent fluorenyl groups (d_{avg} = 3.649 Å) approaches the threshold defined by the sum of the van der Waals radii for Bi and C atoms ($\Sigma d(\mathrm{Bi–C})_{\text{van der Waals}}$ radii = 3.77 Å).

Although the majority of the signals for bismuthinidenes **88**, **90a**, **90b**, and **92** appear within the expected region of the NMR spectra characteristic of diamagnetic compounds and are similar to those of the corresponding Bi(III) precursors, distinct irregular shifts were observed in certain ^{1}H and ^{13}C{^{1}H} NMR signals. The comparative shielding and deshielding effects for the discussed resonances are presented in Table 4. In stark contrast to conventional paramagnetic compounds,

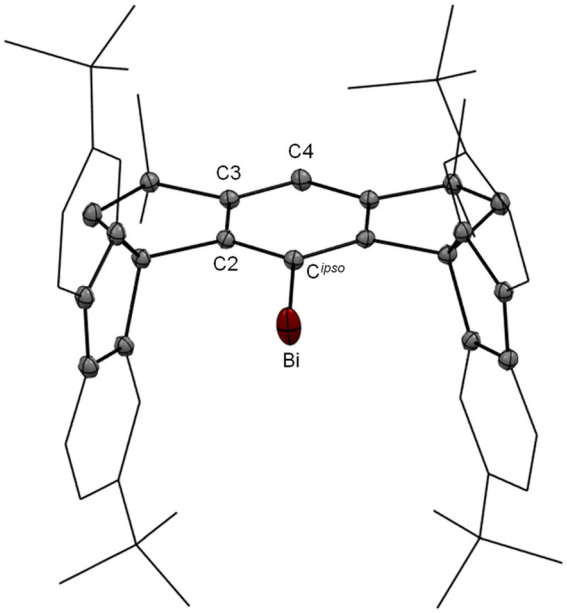

Fig. 9 Molecular structure of triplet ground-state bismuthinidene **88**, reproduced from ref. 143 with permission from the American Association for the Advancement of Science (AAAS), copyright © 2023.

the NMR spectra of all bismuthinidenes are characterized by remarkably sharp signals, with the sole exception of C^{ipso}, whose line broadening arises due to interactions with the quadrupolar ^{209}Bi nuclei.

The SQUID magnetometer did not detect paramagnetic susceptibility for powder samples of the discussed bismuthinidenes **88**, **90a**, and **90b** in the temperature range of 0 to 300 K. This observation suggests that the $M_S = 0$ magnetic sublevel dominates the Boltzmann population, even at room temperature. In a nutshell, these findings indicate that bismuthinidenes possess an $S = 1$ triplet ground state, consistent with the behaviour of integer-spin systems, which typically remain undetectable *via* conventional X-band EPR spectrometers. Quantum chemical calculations were performed on a truncated model of bismuthinidene $\mathbf{90a_{model}}$[144] (where H was replaced by Me on the supporting ligand), which revealed that the triplet state features the leading electronic configuration and the open- and closed-shell singlet states are 76.9 kJ mol^{-1} and 77.3 kJ mol^{-1} higher in energy, respectively (Fig. 11). Accordingly, the nearly degenerate $5p_x$ and $5p_y$ orbitals contribute equally to the total spin population, resulting in a donut-like spin density around the Bi center (spin population = 2.03*e*). Theoretical calculations have predicted that $\mathbf{90a_{model}}$

Table 3 Comparison of selected spectroscopic parameters of condensed-phase pnictinidenes R–Pn (Pn = P–Bi) discussed in this review article

Compound	Spin state	EPR activity	g_{iso}	ZFS (D)/cm^{-1}	E/D
(Phosphino)phosphinidene (**55**)[106]	Singlet	Inactive	—	—	—
M^{S}Fluind*Sb (**79**)[130]	Triplet	Inactive	2.0[a] 1.96[b]	(1030 ± 20)[a] 940[b]	0 0.02[b]
M^{S}Fluind$^{t\mathrm{Bu}}$Bi (**88**)[143]	Triplet	Inactive	—	4523[c] 5422[d]	0.05[c] <0.01[d]
M^{S}Fluind*Bi (**90a**)[144]	Triplet	Inactive	—	>4300[e]	—
Ar*Bi (**92**)[145]	Triplet	Inactive	—	>4100	—

[a] Obtained from simulation of SQUID magnetometric data. [b] Obtained from *ab initio* calculations on a truncated model triplet-state stibinidene. [c] Obtained from *ab initio* calculations. [d] Direct determination by electron paramagnetic resonance using magneto-optical infrared spectroscopy, as described in ref. 150. [e] Obtained from *ab initio* calculations.

Table 4 Abnormal shielding–deshielding behaviour of the aromatic C and H centers close to Bi in the ^{13}C and ^{1}H NMR spectra of the isolated triplet-state bismuthinidenes.[143–145]

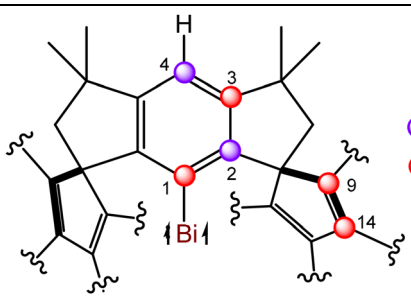

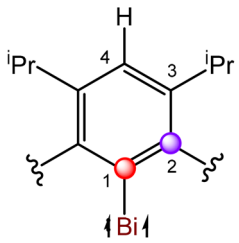

	^{13}C{^{1}H} NMR[a,b]/ppm				^{1}H NMR[a,b]/ppm
Compound	C1	C2	C3	C4	H_{para}
88[a]	−203.8	234	114.5	160.0	−1.06
90a[a]	−203.5	217.7	114.7	160.2	−1.06
90b[b]	−189.5	228.5	114.9	157.3	−0.63
92[b]	−194.7	231.6	—	—	−1.41

[a] (D_8)THF, 298 K. [b] (D_6)benzene, 298 K.

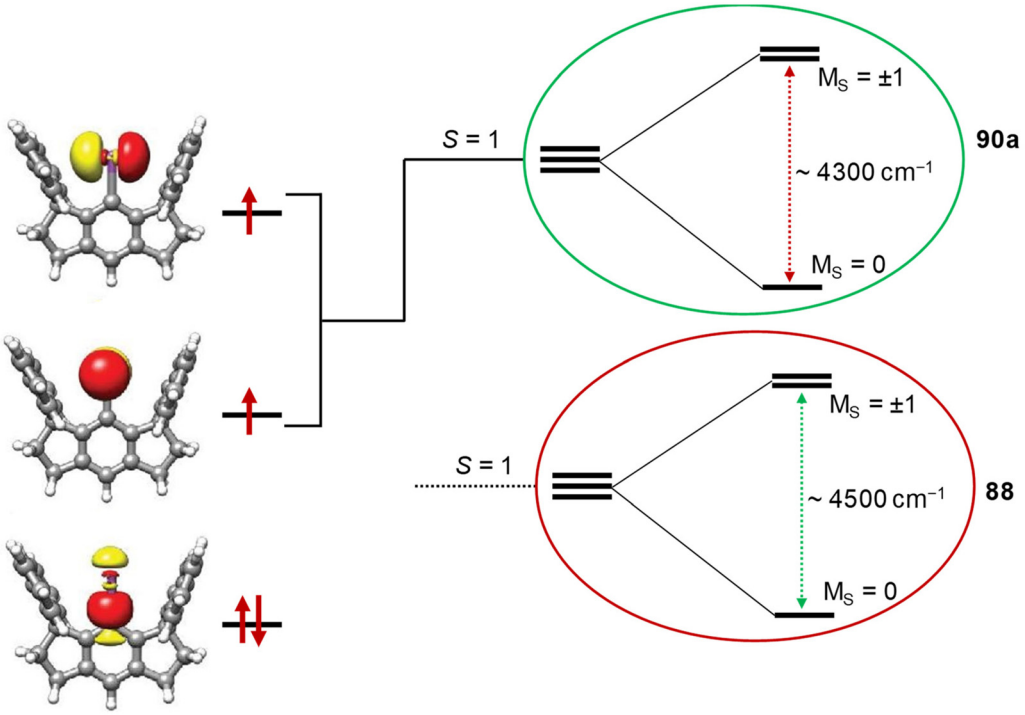

Fig. 10 Electronic structure of **90a**; the central Bi(I) features four electrons in the 6p shell. The three magnetic sublevels of the triplet ground state are split by very large bismuth spin–orbit coupling, which leads to a thermally isolated M_S = 0 level, lowest in energy for Cornella's **88** (red circle) and Tan's **90a** (green circle) bismuthinidenes.[143,144]

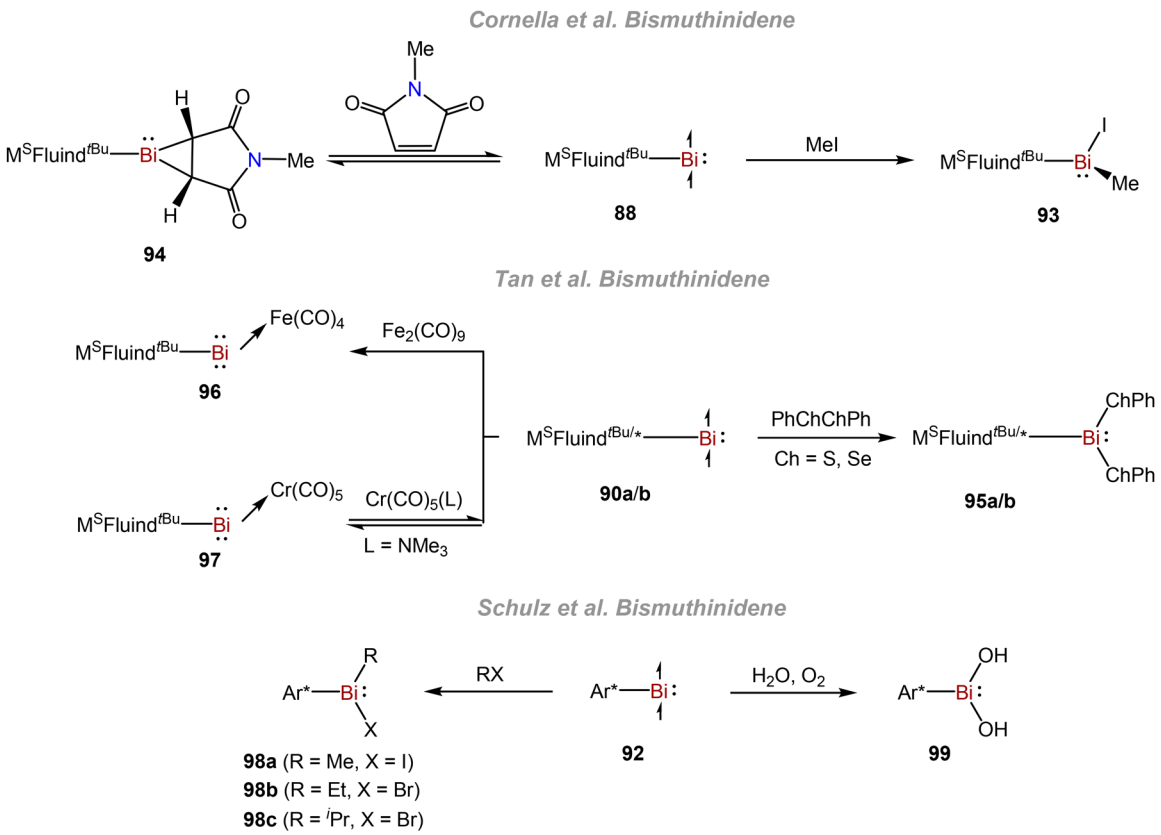

Scheme 19 Reactivity studies of triplet-state bismuthinidenes **88**, **90a/b**, and **92**.[143–145]

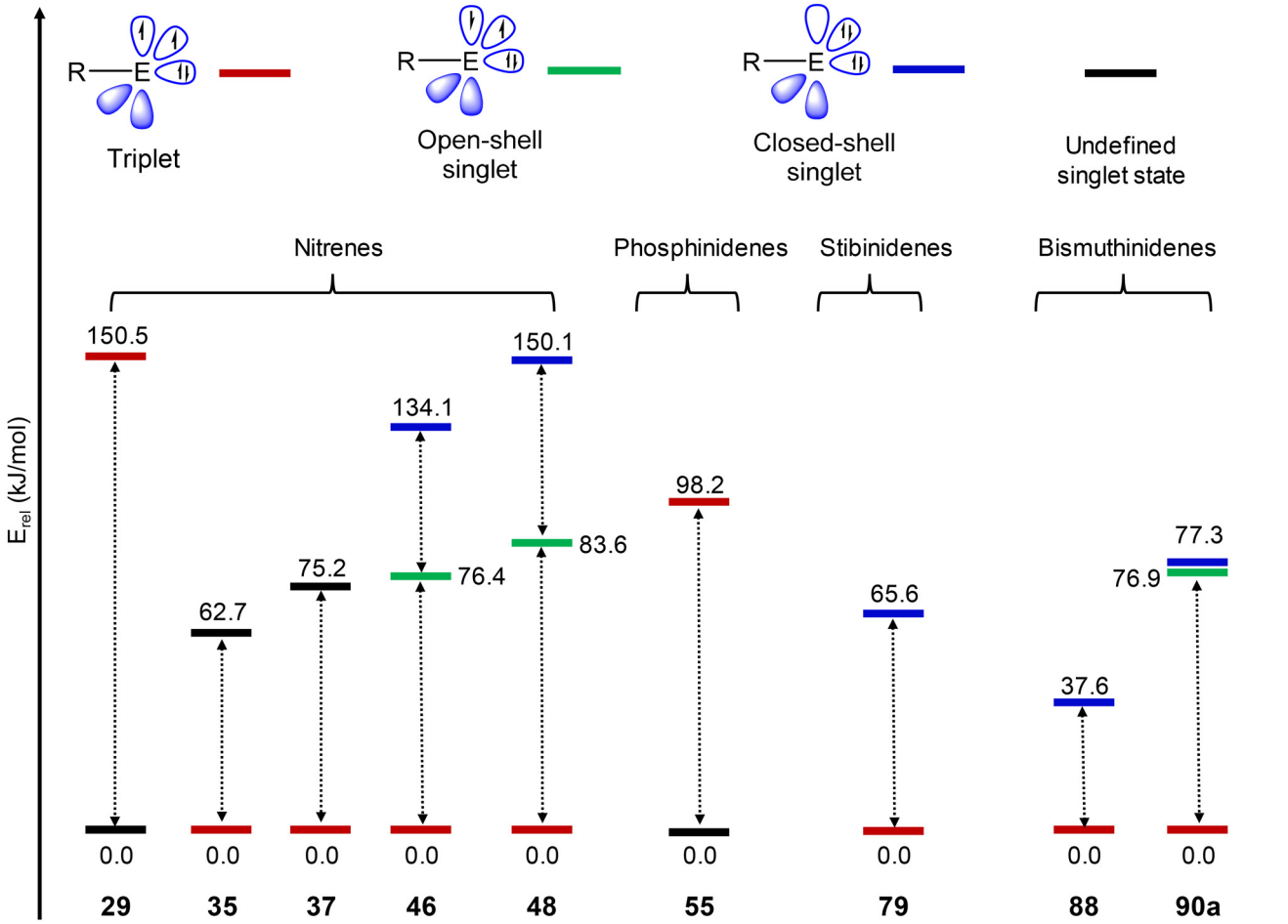

Fig. 11 A pictorial depiction of the electronic states (relative energies in kJ mol^{-1}) on the potential energy hypersurface (PES) is presented for condensed-phase nitrenes (**29**,[7] **46**,[82] and **48**[83]), metallonitrenes (**35**[80] and **37**[81]), phosphinidene (**55**[106]), stibinidene (**79**[130]), and bismuthinidenes (**88**[143] and **90a**[144]), as discussed within this review. The theoretical calculations used the following levels of theory: M05-2X/TZVPP (**29**), CASSCF/NEVPT2 (**35**, **37**, **46**, **48**, **79**, **88** & **90a**), and M06-2X/def2-SVP (**55**).

shows a zero-field splitting of $D > 4300$ cm^{-1}. Such a large and positive ZFS value naturally inclines the system to occupy the energetically lowest-lying, non-magnetic $M_S = 0$ state under ambient conditions. Consequently, the spin population in the higher-energy and magnetically active $M_S = \pm 1$ states remains nearly negligible (Fig. 10).[144] The magnitude of the D value arises from spin–orbit coupling interactions between the triplet state and nearby closed-shell singlet excited states. Cornella's bismuthinidene **88** also exhibits a triplet ground state and is distinguished by a large zero-field splitting parameter of $D > 4500$ cm^{-1} (Fig. 10). Schnegg and coworkers further validate this finding experimentally by magneto-optical infrared detection of electron paramagnetic resonances and provide direct experimental evidence for a large positive ZFS ($D = 5422$ cm^{-1}) in bismuthinidene **88**.[150] However, the experimentally determined D value exceeds theoretical predictions by approximately 20% (Table 3).

The reactivity of the Bi center in bismuthinidenes **88**, **90a**, **90b**, and **92** highlights its +1 oxidation state. Bismuthinidene **88** undergoes oxidative addition with methyl iodide to afford the Bi(III) complex **93** and also engages in a formal [2 + 1] cycloaddition reaction with *N*-methyl maleimide, affording **94** (Scheme 19).[143] Furthermore, Tan's bismuthinidenes **90a/b** undergo oxidative addition with PhChChPh (Ch = S, Se) at the Bi center, yielding oxidative addition products **95a/b**. The triplet ground-state bismuthinidene **90a** also forms stable adducts with $Fe(CO)_4$ (**96**) and $Cr(CO)_5$ (**97**) under ambient conditions (Scheme 19).[144] Bismuthinidene **92** undergoes an oxidation reaction with moist air to selectively afford Ar*Bi(OH)$_2$ (**99**) and reacts with various alkyl halides *via* oxidative addition to give Bi(III) derivatives (**98a–c**) (Scheme 19).[145]

4. Conclusion

In conclusion, this review article outlines how low-valent monocoordinated nitrogen (R–N) and heavier pnictogens (R–Pn, Pn = P–Bi) have flourished over the past two decades, after a prolonged phase of dormancy in the field. The advent of

innovative synthetic methodologies, cutting-edge spectroscopic techniques, and state-of-the-art computational analyses has profoundly advanced the comprehensive understanding of condensed-phase nitrenes and heavier pnictinidenes. The isolation of a "bottleable" singlet-state (phosphino)nitrene and phosphinidene by Bertrand and coworkers has reignited hope for accessing these previously elusive intermediates, which had been accessible only under matrix-isolation conditions. Additionally, sterically bulky hydrindacene ligands have facilitated the isolation of nitrenes and heavier pnictinidenes in their triplet state. At the same time, the introduction of pincer-type PNP scaffolds has enabled the characterization of triplet-state metallonitrenes through photocrystallography. Coincidentally, while this work was under review, a review article by Tan and coworkers summarizing recent advances in pseudo-monocoordinate main-group compounds was published.[151] Overall, we believe that this review article offers a general overview of the synthesis, isolation, and characterization of long-sought nitrenes and heavier pnictinidenes while bridging the domains of fundamental synthetic and computational chemistry. It is hardly an overstatement to assert that continued systematic investigations into nitrenes and heavier pnictinidenes, molecules whose elusive yet captivating electronic structures hold the key to transformative insights, constitute one of the most compelling frontiers in main-group element and reactive intermediate chemistry.

Author contributions

All authors contributed to the writing and revision of the manuscript.

Conflicts of interest

The authors declare no conflicts of interest.

Abbreviations

OSS	Open-shell singlet
CSS	Closed-shell singlet
FVP	Flash vacuum pyrolysis
ESR	Electron spin resonance
IR	Infrared
UV-Vis NIR	Ultraviolet–visible–near infrared
ISC	Intersystem crossing
DFT	Density functional theory
SQUID	Superconducting quantum interference device
ZFS	Zero-field splitting
NLMOs	Natural localized molecular orbitals
NAT	Nitrogen atom transfer
EPR	Electron paramagnetic resonance
sc-XRD	Single-crystal X-ray diffraction
NHCs	N-heterocyclic carbenes
NHCPs	N-heterocyclic carbene phosphinidenes
NBO	Natural bond orbital
WBI	Wiberg bond index
NPA	Natural population analysis
NCDs	Norcaradienes
TM	Transition metal
NCI	Non-covalent interaction
CASSCF	Complete active space self-consistent field
NEVPT2	Second-order N-electron valence perturbation theory
PES	Potential energy hypersurface
HOMO	Highest occupied molecular orbital
LUMO	Lowest unoccupied molecular orbital
LED	Light-emitting diode

Data availability

No primary research results, software, or code have been included, and no new data were generated or analysed as part of this review.

Acknowledgements

We thank the Rheinische Friedrich-Wilhelms-Universität Bonn for the financial support of this work.

References

1 *Reactive Intermediate Chemistry*, ed. R. A. Moss, M. S. Platz and M. Jones, Wiley, 1st edn, 2003.
2 M. Soleilhavoup and G. Bertrand, *Chem*, 2020, **6**, 1275–1282.
3 C. Wentrup, *Angew. Chem., Int. Ed.*, 2018, **57**, 11508–11521.
4 L. Dostál, *Coord. Chem. Rev.*, 2017, **353**, 142–158.
5 M. T. Nguyen, A. Van Keer and L. G. Vanquickenborne, *J. Org. Chem.*, 1996, **61**, 7077–7084.
6 E. C. Mitchell, M. E. Wolf, J. M. Turney and H. F. Schaefer, *Chem. – Eur. J.*, 2021, **27**, 14461–14471.
7 F. Dielmann, O. Back, M. Henry-Ellinger, P. Jerabek, G. Frenking and G. Bertrand, *Science*, 2012, **337**, 1526–1528.
8 C. T. Saouma and J. C. Peters, *Coord. Chem. Rev.*, 2011, **255**, 920–937.
9 T. W. Hayton, *Dalton Trans.*, 2010, **39**, 1145–1158.
10 J. F. Berry, *Comments Inorg. Chem.*, 2009, **30**, 28–66.
11 R. Eikey, *Coord. Chem. Rev.*, 2003, **243**, 83–124.
12 B. A. MacKay and M. D. Fryzuk, *Chem. Rev.*, 2004, **104**, 385–402.
13 N. G. Léonard, T. Chantarojsiri, J. W. Ziller and J. Y. Yang, *J. Am. Chem. Soc.*, 2022, **144**, 1503–1508.
14 W.-L. Man, G. Chen, S.-M. Yiu, L. Shek, W.-Y. Wong, W.-T. Wong and T.-C. Lau, *Dalton Trans.*, 2010, **39**, 11163.

15 J.-P. F. Cherry, A. R. Johnson, L. M. Baraldo, Y.-C. Tsai, C. C. Cummins, S. V. Kryatov, E. V. Rybak-Akimova, K. B. Capps, C. D. Hoff, C. M. Haar and S. P. Nolan, *J. Am. Chem. Soc.*, 2001, **123**, 7271–7286.
16 F. H. Stephens, J. S. Figueroa, P. L. Diaconescu and C. C. Cummins, *J. Am. Chem. Soc.*, 2003, **125**, 9264–9265.
17 J. Abbenseth, M. Diefenbach, A. Hinz, L. Alig, C. Würtele, J. M. Goicoechea, M. C. Holthausen and S. Schneider, *Angew. Chem., Int. Ed.*, 2019, **58**, 10966–10970.
18 A. R. Fox, C. R. Clough, N. A. Piro and C. C. Cummins, *Angew. Chem., Int. Ed.*, 2007, **46**, 973–976.
19 J. A. Buss, P. H. Oyala and T. Agapie, *Angew. Chem., Int. Ed.*, 2017, **56**, 14502–14506.
20 J. J. Curley, N. A. Piro and C. C. Cummins, *Inorg. Chem.*, 2009, **48**, 9599–9601.
21 H. A. Spinney, N. A. Piro and C. C. Cummins, *J. Am. Chem. Soc.*, 2009, **131**, 16233–16243.
22 N. C. Mösch-Zanetti, R. R. Schrock, W. M. Davis, K. Wanninger, S. W. Seidel and M. B. O'Donoghue, *J. Am. Chem. Soc.*, 1997, **119**, 11037–11048.
23 G. Balázs, M. Sierka and M. Scheer, *Angew. Chem., Int. Ed.*, 2005, **44**, 4920–4924.
24 M. Yoshifuji, I. Shima, N. Inamoto, K. Hirotsu and T. Higuchi, *J. Am. Chem. Soc.*, 1981, **103**, 4587–4589.
25 L. Weber, F. Ebeler and R. S. Ghadwal, *Coord. Chem. Rev.*, 2022, **461**, 214499.
26 B. Twamley, C. D. Sofield, M. M. Olmstead and P. P. Power, *J. Am. Chem. Soc.*, 1999, **121**, 3357–3367.
27 N. Tokitoh, Y. Arai, R. Okazaki and S. Nagase, *Science*, 1997, **277**, 78–80.
28 L. Tuscher, C. Ganesamoorthy, D. Bläser, C. Wölper and S. Schulz, *Angew. Chem., Int. Ed.*, 2015, **54**, 10657–10661.
29 L. Tuscher, C. Helling, C. Ganesamoorthy, J. Krüger, C. Wölper, W. Frank, A. S. Nizovtsev and S. Schulz, *Chem. – Eur. J.*, 2017, **23**, 12297–12304.
30 H. M. Weinert, C. Wölper and S. Schulz, *Organometallics*, 2021, **40**, 3486–3495.
31 J. Krüger, C. Wölper, A. A. Auer and S. Schulz, *Eur. J. Inorg. Chem.*, 2022, **2022**, e202100960.
32 D. Dange, A. Davey, J. A. B. Abdalla, S. Aldridge and C. Jones, *Chem. Commun.*, 2015, **51**, 7128–7131.
33 M. Sakagami, T. Sasamori, H. Sakai, Y. Furukawa and N. Tokitoh, *Chem. – Asian J.*, 2013, **8**, 690–693.
34 L. P. Ho, A. Nasr, P. G. Jones, A. Altun, F. Neese, G. Bistoni and M. Tamm, *Chem. – Eur. J.*, 2018, **24**, 18922–18932.
35 N. Tokitoh, Y. Arai, T. Sasamori, R. Okazaki, S. Nagase, H. Uekusa and Y. Ohashi, *J. Am. Chem. Soc.*, 1998, **120**, 433–434.
36 A. H. Cowley, *Acc. Chem. Res.*, 1997, **30**, 445–451.
37 P. Šimon, F. de Proft, R. Jambor, A. Růžička and L. Dostál, *Angew. Chem., Int. Ed.*, 2010, **49**, 5468–5471.
38 M. M. Siddiqui, S. K. Sarkar, M. Nazish, M. Morganti, C. Köhler, J. Cai, L. Zhao, R. Herbst-Irmer, D. Stalke, G. Frenking and H. W. Roesky, *J. Am. Chem. Soc.*, 2021, **143**, 1301–1306.
39 Y. Pang, M. Leutzsch, N. Nöthling, F. Katzenburg and J. Cornella, *J. Am. Chem. Soc.*, 2021, **143**, 12487–12493.
40 R. Kretschmer, D. A. Ruiz, C. E. Moore, A. L. Rheingold and G. Bertrand, *Angew. Chem., Int. Ed.*, 2014, **53**, 8176–8179.
41 G. Dequirez, V. Pons and P. Dauban, *Angew. Chem., Int. Ed.*, 2012, **51**, 7384–7395.
42 F. Tiemann, *Ber. Dtsch. Chem. Ges.*, 1891, **24**, 4162–4167.
43 D. M. Meyer and K. C. Roth, *Astrophys. J.*, 1991, **376**, L49.
44 N. P. Gritsan and M. S. Platz, *Chem. Rev.*, 2006, **106**, 3844–3867.
45 *Organic Azides: Syntheses and Applications*, ed. S. Bräse and K. Banert, Wiley, 1st edn, 2009.
46 M. Kuzaj, H. Lüerssen and C. Wentrup, *Angew. Chem., Int. Ed. Engl.*, 1986, **25**, 480–482.
47 Z. Wu, H. Li, B. Zhu, X. Zeng, S. A. Hayes, N. W. Mitzel, H. Beckers and R. J. F. Berger, *Phys. Chem. Chem. Phys.*, 2015, **17**, 8784–8791.
48 *Nitrenes: Reactive Intermediates in Organic Chemistry*, ed. W. Lwowski, Inter Science Pub., New York, 1970.
49 D. Li, H. Li, B. Zhu, X. Zeng, H. Willner, H. Beckers, P. Neuhaus, D. Grote and W. Sander, *Phys. Chem. Chem. Phys.*, 2015, **17**, 6433–6439.
50 X. Zeng, H. Beckers, H. Willner, P. Neuhaus, D. Grote and W. Sander, *Chem. – Eur. J.*, 2009, **15**, 13466–13473.
51 H. Li, Z. Wu, D. Li, X. Zeng, H. Beckers and J. S. Francisco, *J. Am. Chem. Soc.*, 2015, **137**, 10942–10945.
52 X. Zeng, H. Beckers, P. Neuhaus, D. Grote and W. Sander, *Z. Anorg. Allg. Chem.*, 2012, **638**, 526–533.
53 X. Zeng, H. Beckers and H. Willner, *J. Am. Chem. Soc.*, 2013, **135**, 2096–2099.
54 X. Zeng, H. Beckers and H. Willner, *Angew. Chem., Int. Ed.*, 2013, **52**, 7981–7984.
55 X. Zeng, H. Beckers, H. Willner, P. Neuhaus, D. Grote and W. Sander, *J. Phys. Chem. A*, 2015, **119**, 2281–2288.
56 G. Deng, X. Dong, Q. Liu, D. Li, H. Li, Q. Sun and X. Zeng, *Phys. Chem. Chem. Phys.*, 2017, **19**, 3792–3799.
57 Z. Wu, D. Li, H. Li, B. Zhu, H. Sun, J. S. Francisco and X. Zeng, *Angew. Chem., Int. Ed.*, 2016, **55**, 1507–1510.
58 M. P. Sherman and W. S. Jenks, *J. Org. Chem.*, 2014, **79**, 8977–8983.
59 H. Sun, B. Zhu, Z. Wu, X. Zeng, H. Beckers and W. S. Jenks, *J. Org. Chem.*, 2015, **80**, 2006–2009.
60 X. Zeng, H. Beckers, H. Willner, D. Grote and W. Sander, *Chem. – Eur. J.*, 2011, **17**, 3977–3984.
61 Q. Liu, H. Li, Z. Wu, D. Li, H. Beckers, G. Rauhut and X. Zeng, *Chem. – Asian J.*, 2016, **11**, 2953–2959.
62 H. Li, Z. Wu, D. Li, H. Wan, J. Xu, M. Abe and X. Zeng, *Chem. Commun.*, 2017, **53**, 4783–4786.
63 H. Wan, J. Xu, Q. Liu, H. Li, Y. Lu, M. Abe and X. Zeng, *J. Phys. Chem. A*, 2017, **121**, 8604–8613.
64 H. Li, H. Wan, Z. Wu, D. Li, D. Bégué, C. Wentrup and X. Zeng, *Chem. – Eur. J.*, 2016, **22**, 7856–7862.
65 H. Wan, H. Li, J. Xu, Z. Wu, Q. Liu, X. Chu, M. Abe, D. Bégué and X. Zeng, *Org. Chem. Front.*, 2017, **4**, 1839–1848.

66 A. J. Arduengo, R. L. Harlow and M. Kline, *J. Am. Chem. Soc.*, 1991, **113**, 361–363.
67 V. Lavallo, J. Mafhouz, Y. Canac, B. Donnadieu, W. W. Schoeller and G. Bertrand, *J. Am. Chem. Soc.*, 2004, **126**, 8670–8671.
68 W. D. Hinsberg and P. B. Dervan, *J. Am. Chem. Soc.*, 1978, **100**, 1608–1610.
69 P. G. Schultz and P. B. Dervan, *J. Am. Chem. Soc.*, 1980, **102**, 878–880.
70 W. D. Hinsberg, P. G. Schultz and P. B. Dervan, *J. Am. Chem. Soc.*, 1982, **104**, 766–773.
71 P. B. Dervan, M. E. Squillacote, P. M. Lahti, A. P. Sylwester and J. D. Roberts, *J. Am. Chem. Soc.*, 1981, **103**, 1120–1122.
72 W. Schoeller and A. B. Rozhenko, *Eur. J. Inorg. Chem.*, 2001, **2001**, 845–850.
73 C. B. Caputo, L. J. Hounjet, R. Dobrovetsky and D. W. Stephan, *Science*, 2013, **341**, 1374–1377.
74 O. Back, B. Donnadieu, M. Von Hopffgarten, S. Klein, R. Tonner, G. Frenking and G. Bertrand, *Chem. Sci.*, 2011, **2**, 858.
75 B. E. Maryanoff, *Heteroat. Chem.*, 1993, **4**, 105.
76 H. B. Gray and J. R. Winkler, *Acc. Chem. Res.*, 2018, **51**, 1850–1857.
77 *Progress in Inorganic Chemistry*, Wiley, 1st edn, 2014, pp. 417–470.
78 K. M. Carsch, I. M. DiMucci, D. A. Iovan, A. Li, S.-L. Zheng, C. J. Titus, S. J. Lee, K. D. Irwin, D. Nordlund, K. M. Lancaster and T. A. Betley, *Science*, 2019, **365**, 1138–1143.
79 C. G. Werncke, *Dalton Trans.*, 2025, **54**, 8374–8384.
80 J. Sun, J. Abbenseth, H. Verplancke, M. Diefenbach, B. De Bruin, D. Hunger, C. Würtele, J. Van Slageren, M. C. Holthausen and S. Schneider, *Nat. Chem.*, 2020, **12**, 1054–1059.
81 T. Schmidt-Räntsch, H. Verplancke, J. N. Lienert, S. Demeshko, M. Otte, G. P. Van Trieste, K. A. Reid, J. H. Reibenspies, D. C. Powers, M. C. Holthausen and S. Schneider, *Angew. Chem., Int. Ed.*, 2022, **61**, e202115626.
82 M. Janssen, T. Frederichs, M. Olaru, E. Lork, E. Hupf and J. Beckmann, *Science*, 2024, **385**, 318–321.
83 D. Wang, W. Chen, H. Chen, Y. Chen, S. Ye and G. Tan, *Nat. Chem.*, 2025, **17**, 38–43.
84 T. Matsuo, K. Suzuki, T. Fukawa, B. Li, M. Ito, Y. Shoji, T. Otani, L. Li, M. Kobayashi, M. Hachiya, Y. Tahara, D. Hashizume, T. Fukunaga, A. Fukazawa, Y. Li, H. Tsuji and K. Tamao, *Bull. Chem. Soc. Jpn.*, 2011, **84**, 1178–1191.
85 M. Olaru, S. Mebs and J. Beckmann, *Angew. Chem., Int. Ed.*, 2021, **60**, 19133–19138.
86 Y. He, C. Dai, D. Wang, J. Zhu and G. Tan, *J. Am. Chem. Soc.*, 2022, **144**, 5126–5135.
87 M. Janssen, S. Mebs and J. Beckmann, *ChemPlusChem*, 2023, **88**, e202200429.
88 D. Wang, C. Zhai, Y. Chen, Y. He, X. Chen, S. Wang, L. Zhao, G. Frenking, X. Wang and G. Tan, *Nat. Chem.*, 2023, **15**, 200–205.
89 H. Chen, W. Chen, D. Wang, Y. Chen, Z. Liu, S. Ye, G. Tan and S. Gao, *Angew. Chem., Int. Ed.*, 2024, **63**, e202402093.
90 D. Wang, W. Chen, C. Zhai, L. Zhao, S. Ye and G. Tan, *J. Am. Chem. Soc.*, 2023, **145**, 6914–6920.
91 P. Biegger, M. Schaffroth, K. Brödner, O. Tverskoy, F. Rominger and U. H. F. Bunz, *Chem. Commun.*, 2015, **51**, 14844–14847.
92 A. Grünwald, B. Goswami, K. Breitwieser, B. Morgenstern, M. Gimferrer, F. W. Heinemann, D. M. Momper, C. W. M. Kay and D. Munz, *J. Am. Chem. Soc.*, 2022, **144**, 8897–8901.
93 H. Stafford, T. M. Rookes, E. P. Wildman, G. Balázs, A. J. Wooles, M. Scheer and S. T. Liddle, *Angew. Chem., Int. Ed.*, 2017, **56**, 7669–7673.
94 M. B. Geeson, W. J. Transue and C. C. Cummins, *J. Am. Chem. Soc.*, 2019, **141**, 13336–13340.
95 B. Feng, L. Xiang, A. Carpentier, L. Maron, X. Leng and Y. Chen, *J. Am. Chem. Soc.*, 2021, **143**, 2705–2709.
96 T. L. Breen and D. W. Stephan, *J. Am. Chem. Soc.*, 1995, **117**, 11914–11921.
97 L. Weber, *Chem. Rev.*, 1992, **92**, 1839–1906.
98 K. Lammertsma, in *New Aspects in Phosphorus Chemistry III*, ed. J.-P. Majoral, Springer Berlin Heidelberg, Berlin, Heidelberg, 2003, vol. 229, pp. 95–119.
99 F. Mathey, *Angew. Chem., Int. Ed.*, 2003, **42**, 1578–1604.
100 R. Waterman, *Chem*, 2016, **1**, 27–29.
101 Z. Benkő, R. Streubel and L. Nyulászi, *Dalton Trans.*, 2006, 4321–4327.
102 S. Gronert, J. R. Keeffe and R. A. M. O'Ferrall, *J. Am. Chem. Soc.*, 2011, **133**, 3381–3389.
103 H. Zhu and S. Inoue, *Chem*, 2025, **11**, 102649.
104 B. Lu and X. Zeng, *Chem. – Eur. J.*, 2024, **30**, e202303283.
105 S. Quek, R. Ishizeki, Z.-F. Zhang, M.-D. Su, R. K. Siwatch and C.-W. So, *Inorg. Chem.*, 2025, **64**, 23255–23262.
106 L. Liu, D. A. Ruiz, D. Munz and G. Bertrand, *Chem*, 2016, **1**, 147–153.
107 M. M. Hansmann, R. Jazzar and G. Bertrand, *J. Am. Chem. Soc.*, 2016, **138**, 8356–8359.
108 Y. Chen, P. Su, D. Wang, Z. Ke and G. Tan, *Nat. Commun.*, 2024, **15**, 4579.
109 E. Buchner and Th. Curtius, *Ber. Dtsch. Chem. Ges.*, 1885, **18**, 2377–2379.
110 E. Ciganek, *J. Am. Chem. Soc.*, 1967, **89**, 1454–1458.
111 L. Weber, O. Kaminski, H. Stammler and B. Neumann, *Chem. Ber.*, 1996, **129**, 223–226.
112 L. Weber, *Eur. J. Inorg. Chem.*, 2007, **2007**, 4095–4117.
113 A. J. Arduengo, J. C. Calabrese, A. H. Cowley, H. V. R. Dias, J. R. Goerlich, W. J. Marshall and B. Riegel, *Inorg. Chem.*, 1997, **36**, 2151–2158.
114 R. C. Smith, P. Gantzel, A. L. Rheingold and J. D. Protasiewicz, *Organometallics*, 2004, **23**, 5124–5126.
115 B. A. Chalmers, M. Bühl, K. S. A. Arachchige, A. M. Z. Slawin and P. Kilian, *J. Am. Chem. Soc.*, 2014, **136**, 6247–6250.
116 L. J. Taylor, M. Bühl, P. Wawrzyniak, B. A. Chalmers, J. D. Woollins, A. M. Z. Slawin, A. L. Fuller and P. Kilian, *Eur. J. Inorg. Chem.*, 2016, **2016**, 659–666.
117 C. Präsang, M. Stoelzel, S. Inoue, A. Meltzer and M. Driess, *Angew. Chem., Int. Ed.*, 2010, **49**, 10002–10005.

118 S. Yao, Y. Grossheim, A. Kostenko, E. Ballestero-Martínez, S. Schutte, M. Bispinghoff, H. Grützmacher and M. Driess, *Angew. Chem., Int. Ed.*, 2017, **56**, 7465–7469.
119 G. Reeske and A. H. Cowley, *Chem. Commun.*, 2006, 1784.
120 J. Zechovský, E. Kertész, V. Kremláček, M. Hejda, T. Mikysek, M. Erben, A. Růžička, R. Jambor, Z. Benkő and L. Dostál, *Organometallics*, 2022, **41**, 2535–2550.
121 F. Meyer, A. Siumbeli, L. Dostál, E. Hupf and J. Beckmann, *Chem. Sci.*, 2025, **16**, 16232–16239.
122 C. L. Dorsey, R. M. Mushinski and T. W. Hudnall, *Chem. – Eur. J.*, 2014, **20**, 8914–8917.
123 B. Sigwarth, U. Weber, L. Zsolnai and G. Huttner, *Chem. Ber.*, 1985, **118**, 3114–3126.
124 J. Von Seyerl and G. Huttner, *Angew. Chem., Int. Ed. Engl.*, 1978, **17**, 843–844.
125 A. H. Cowley, N. C. Norman and M. Pakulski, *J. Am. Chem. Soc.*, 1984, **106**, 6844–6845.
126 A. H. Cowley, N. C. Norman, M. Pakulski, D. Bricker and D. R. Russell, *J. Am. Chem. Soc.*, 1985, **107**, 8211–8218.
127 A. H. Cowley, *Phosphorous Sulfur Relat. Elem.*, 1986, **26**, 31–38.
128 A. M. Arif, A. H. Cowley, N. C. Norman and M. Pakulski, *Inorg. Chem.*, 1986, **25**, 4836–4840.
129 R. Waterman and T. D. Tilley, *Chem. Commun.*, 2006, 4030–4032.
130 M. Wu, H. Li, W. Chen, D. Wang, Y. He, L. Xu, S. Ye and G. Tan, *Chem*, 2023, **9**, 2573–2584.
131 Y. Pang, M. Leutzsch, N. Nöthling and J. Cornella, *Angew. Chem., Int. Ed.*, 2023, **62**, e202302071.
132 S. P. Green, C. Jones and A. Stasch, *Science*, 2007, **318**, 1754–1757.
133 B. Twamley, C.-S. Hwang, N. J. Hardman and P. P. Power, *J. Organomet. Chem.*, 2000, **609**, 152–160.
134 E. R. Johnson, S. Keinan, P. Mori-Sánchez, J. Contreras-García, A. J. Cohen and W. Yang, *J. Am. Chem. Soc.*, 2010, **132**, 6498–6506.
135 A. Schnegg, in *eMagRes*, ed. R. K. Harris and R. L. Wasylishen, John Wiley & Sons, Ltd, Chichester, UK, 2017, pp. 115–132.
136 A. Velian and C. C. Cummins, *J. Am. Chem. Soc.*, 2012, **134**, 13978–13981.
137 H. Jansen, M. C. Samuels, E. P. A. Couzijn, J. C. Slootweg, A. W. Ehlers, P. Chen and K. Lammertsma, *Chem. – Eur. J.*, 2010, **16**, 1454–1458.
138 J. B. M. Wit, G. B. De Jong, M. Schakel, M. Lutz, A. W. Ehlers, J. C. Slootweg and K. Lammertsma, *Organometallics*, 2016, **35**, 1170–1176.
139 A. Heimer and E. Hulthén, *Nature*, 1931, **127**, 557.
140 G. Herzberg, *Molecular Spectra and Molecular Structure – Vol I*, Read Books Ltd, 2013.
141 D. P. Mukhopadhyay, D. Schleier, S. Wirsing, J. Ramler, D. Kaiser, E. Reusch, P. Hemberger, T. Preitschopf, I. Krummenacher, B. Engels, I. Fischer and C. Lichtenberg, *Chem. Sci.*, 2020, **11**, 7562–7568.
142 H. J. Breunig, R. Rösler and E. Lork, *Angew. Chem., Int. Ed.*, 1998, **37**, 3175–3177.
143 Y. Pang, N. Nöthling, M. Leutzsch, L. Kang, E. Bill, M. Van Gastel, E. Reijerse, R. Goddard, L. Wagner, D. SantaLucia, S. DeBeer, F. Neese and J. Cornella, *Science*, 2023, **380**, 1043–1048.
144 M. Wu, W. Chen, D. Wang, Y. Chen, S. Ye and G. Tan, *Natl. Sci. Rev.*, 2023, **10**, nwad169.
145 Y. Schulte, T. Freese, C. Wölper, J. Schulte, G. Haberhauer and S. Schulz, *Angew. Chem., Int. Ed.*, 2025, **64**, e202508250.
146 P. Pyykkö and M. Atsumi, *Chem. – Eur. J.*, 2009, **15**, 186–197.
147 G. Wang, L. A. Freeman, D. A. Dickie, R. Mokrai, Z. Benkő and R. J. Gilliard, *Chem. – Eur. J.*, 2019, **25**, 4335–4339.
148 I. Vránová, M. Alonso, R. Lo, R. Sedlák, R. Jambor, A. Růžička, F. D. Proft, P. Hobza and L. Dostál, *Chem. – Eur. J.*, 2015, **21**, 16917–16928.
149 Y. Pang, M. Leutzsch, N. Nöthling and J. Cornella, *J. Am. Chem. Soc.*, 2020, **142**, 19473–19479.
150 T. Al Said, D. Spinnato, K. Holldack, F. Neese, J. Cornella and A. Schnegg, *J. Am. Chem. Soc.*, 2025, **147**, 84–87.
151 G. Tan and S. Ye, *Acc. Chem. Res.*, 2026, **59**, 397–410.